

# Inclusive neutrino scattering off deuteron from threshold to GeV energies

G. Shen<sup>a</sup>, L.E. Marcucci<sup>b,c</sup>, J. Carlson<sup>a</sup>, S. Gandolfi<sup>a</sup>, and R. Schiavilla<sup>d,e</sup>

<sup>a</sup>*Theoretical Division, Los Alamos National Laboratory, NM 87545, USA*

<sup>b</sup>*Department of Physics, University of Pisa, 56127 Pisa, Italy*

<sup>c</sup>*INFN-Pisa, 56127 Pisa, Italy*

<sup>d</sup>*Department of Physics, Old Dominion University, Norfolk, VA 23529, USA*

<sup>e</sup>*Jefferson Lab, Newport News, VA 23606, USA*

(Dated: October 16, 2018)

Background: Neutrino-nucleus quasi-elastic scattering is crucial to interpret the neutrino oscillation results in long baseline neutrino experiments. There are rather large uncertainties in the cross section, due to insufficient knowledge on the role of two-body weak currents. Purpose: Determine the role of two-body weak currents in neutrino-deuteron quasi-elastic scattering up to GeV energies. Methods: Calculate cross sections for inclusive neutrino scattering off deuteron induced by neutral and charge-changing weak currents, from threshold up to GeV energies, using the Argonne  $v_{18}$  potential and consistent nuclear electroweak currents with one- and two-body terms. Results: Two-body contributions are found to be small, and increase the cross sections obtained with one-body currents by less than 10% over the whole range of energies. Total cross sections obtained by describing the final two-nucleon states with plane waves differ negligibly, for neutrino energies  $\gtrsim 500$  MeV, from those in which interaction effects in these states are fully accounted for. The sensitivity of the calculated cross sections to different models for the two-nucleon potential and/or two-body terms in the weak current is found to be weak. Comparing cross sections to those obtained in a naive model in which the deuteron is taken to consist of a free proton and neutron at rest, nuclear structure effects are illustrated to be non-negligible. Conclusion: Contributions of two-body currents in neutrino-deuteron quasi-elastic scattering up to GeV are found to be smaller than 10%. Finally, it should be stressed that the results reported in this work do not include pion production channels.

PACS numbers: 25.10.+s, 25.30.Pt

## I. INTRODUCTION

In last few years, inclusive neutrino scattering from nuclear targets has become a hot topic. Interest has been spurred by the anomaly observed in recent neutrino quasi-elastic scattering data on  $^{12}\text{C}$  [1, 2], i.e. the excess, at relatively low energy, of measured cross section relative to theoretical calculations. Analyses based on these calculations have led to speculations that our present understanding of the nuclear response to charge-changing weak probes may be incomplete [3], and, in particular, that the momentum transfer dependence of the axial form factor of the nucleon, specifically the cutoff value of its dipole parameterization [4], may be quite different from that obtained from analyses of pion electro-production data [5] and measurements of the reaction  $n(\nu_\mu, \mu^-)p$  in the deuteron at quasi-elastic kinematics [6, 7] and of  $\nu_\mu p$  and  $\bar{\nu}_\mu p$  elastic scattering [8] ( $\Lambda_A \simeq 1.20$  GeV versus  $\Lambda_A \simeq 1$  GeV). However, it should be emphasized that the calculations on which these analyses are based use rather crude models of nuclear structure—Fermi gas or local density approximations of the nuclear matter spectral function—as well as simplistic treatments of the reaction mechanism, and should therefore be viewed with skepticism.

In this paper, we calculate cross sections for inclusive neutrino scattering off deuteron in a wide energy range, from threshold up to 1 GeV. The motivations for undertaking such a work are twofold. The first is to provide a benchmark for studies of electro-weak inclusive response in light nuclei we intend to carry out in the near future. The second motivation has to do with plans [9], still under development, to determine the neutrino flux in accelerator-based experiments from measurements of inclusive cross sections on the deuteron. In particular, in charged-current neutrino capture on deuteron, the final states  $ppl^-$  can be measured, in principle, very well. Clearly, accurate predictions for these cross sections are crucial for a reliable determination of the flux.

A number of studies of neutrino-deuteron scattering at low and intermediate energies ( $\lesssim 150$  MeV) were carried out in the past decades, see Ref. [10] for a review of work done up to the mid 1990's. These efforts culminated in the Nakamura *et al.*'s 2001 and 2002 calculations of the cross sections for neutrino disintegration of the deuteron induced by neutral and charge-changing weak currents. These calculations were based on bound- and scattering-state wave functions obtained from last-generation realistic potentials, and used a realistic model for the nuclear weak current, including one- and two-body terms. The vector part of this current was shown to provide an excellent description of the  $np$  radiative capture cross section for neutron energies up to 100 MeV [11], while the axial part was constrained to reproduce the Gamow-Teller matrix element in tritium  $\beta$ -decay [12]. The Nakamura *et al.* studies have played

an important role in the analysis and interpretation of the Sudbury Neutrino Observatory (SNO) experiments [13], which have established solar neutrino oscillations and the validity of the standard model for the generation of energy and neutrinos in the sun [14].

In the present work, we use the same theoretical framework as the authors of Refs. [11, 12], but include refinements in the modeling of the weak current—which however, as shown in Sec. V, will turn out to have a minor impact on the predicted cross sections—and extend the range of neutrino energies up to 1 GeV. While the theoretical approach is essentially the same, nevertheless the way in which the calculations are carried out in practice is rather different from that used in those earlier papers, which relied on a multipole expansion of the weak transition operators, and evaluated the cross section by summing over a relatively large number of final two-nucleon channels states. In contrast, we evaluate, by direct numerical integrations, the matrix elements of the weak current between the deuteron and the two-nucleon scattering states labeled by the relative momentum  $\mathbf{p}$  (and in given pair spin and isospin channels), thus avoiding cumbersome multipole expansions. Differential cross sections are then obtained by integrating over  $\mathbf{p}$  (and summing over the discrete quantum numbers) appropriate combinations of these matrix elements, i.e. by calculating the weak response functions. The techniques developed here for the deuteron should prove valuable when we will attempt the Green's function Monte Carlo calculation of these response functions (or rather, their Laplace transforms [15]) in  $A > 2$  nuclei.

This paper is organized as follows. In Sec. II and Appendix A we present the neutrino and antineutrino differential cross sections expressed in terms of response functions, while in Sec. III we provide a succinct description of the neutral and charge-changing weak-current model. In Sec. IV we outline the methods used to obtain the two-nucleon bound and continuum states, and discuss the numerical evaluation of the response functions. A variety of results for the neutral current processes  ${}^2\text{H}(\nu_l, \nu_l)pn$  and  ${}^2\text{H}(\bar{\nu}_l, \bar{\nu}_l)pn$ , and charge-changing processes  ${}^2\text{H}(\nu_e, e^-)pp$  and  ${}^2\text{H}(\bar{\nu}_e, e^+)nn$  are presented in Sec. V, including the sensitivity of the calculated cross sections to (i) interaction effects in the final states, (ii) different short-range behaviors of the two-body axial weak currents, and (iii) different potential models to describe the two-nucleon bound and continuum states. In order to illustrate the effects of nuclear structure, we compare these cross sections to those obtained in a naive model in which the deuteron is taken to consist of a free proton and neutron (the free nucleon cross sections are listed for reference in Appendix B). Concluding remarks and an outlook are given in Sec. VI.

## II. INCLUSIVE NEUTRINO SCATTERING OFF DEUTERON

The differential cross section for neutrino ( $\nu$ ) and antineutrino ( $\bar{\nu}$ ) inclusive scattering off deuteron, specifically the processes

$$\nu_l + d \longrightarrow \nu_l + p + n, \quad \bar{\nu}_l + d \longrightarrow \bar{\nu}_l + p + n \quad (2.1)$$

induced by neutral weak currents (NC), and the processes

$$\nu_l + d \longrightarrow l^- + p + p, \quad \bar{\nu}_l + d \longrightarrow l^+ + n + n \quad (2.2)$$

induced by charge-changing weak currents (CC), can be expressed as

$$\begin{aligned} \left( \frac{d\sigma}{d\epsilon' d\Omega} \right)_{\nu/\bar{\nu}} = & \frac{G^2}{2\pi^2} k' \epsilon' F(Z, k') \cos^2 \frac{\theta}{2} \left[ R_{00} + \frac{\omega^2}{q^2} R_{zz} - \frac{\omega}{q} R_{0z} + \left( \tan^2 \frac{\theta}{2} + \frac{Q^2}{2q^2} \right) R_{xx+yy} \right. \\ & \left. \mp \tan \frac{\theta}{2} \sqrt{\tan^2 \frac{\theta}{2} + \frac{Q^2}{q^2}} R_{xy} \right], \end{aligned} \quad (2.3)$$

where  $G=G_F$  for the NC processes and  $G=G_F \cos \theta_C$  for the CC processes, and the  $- (+)$  sign in the last term is relative to the  $\nu (\bar{\nu})$  initiated reactions. Following Ref. [12], we adopt the value  $G_F = 1.1803 \times 10^{-5} \text{ GeV}^{-2}$  as obtained from an analysis of super-allowed  $0^+ \rightarrow 0^+$   $\beta$ -decays [16]—this value includes radiative corrections—while  $\cos \theta_C$  is taken as 0.97425 from [17]. The initial neutrino four-momentum is  $k^\mu = (\epsilon, \mathbf{k})$ , the final lepton four momentum is  $k'^\mu = (\epsilon', \mathbf{k}')$ , and the lepton scattering angle is denoted by  $\theta$ . We have also defined the lepton energy and momentum transfers as  $\omega = \epsilon - \epsilon'$  and  $\mathbf{q} = \mathbf{k} - \mathbf{k}'$ , respectively, and the squared four-momentum transfer as  $Q^2 = q^2 - \omega^2 > 0$ . The Fermi function  $F(Z, k')$  with  $Z = 2$  accounts for the Coulomb distortion of the final lepton wave function in the charge-raising reaction,

$$F(Z, k') = 2(1 + \gamma) (2k' r_d)^{2\gamma-2} \exp(\pi y) \left| \frac{\Gamma(\gamma + i y)}{\Gamma(1 + 2\gamma)} \right|^2, \quad \gamma = \sqrt{1 - (Z\alpha)^2}, \quad (2.4)$$

it is set to one otherwise. Here  $y = Z \alpha \epsilon' / k'$ ,  $\Gamma(z)$  is the gamma function,  $r_d$  is the deuteron radius ( $r_d = 1.967$  fm), and  $\alpha$  is the fine structure constant. Radiative corrections for the CC and NC processes due to bremsstrahlung and virtual photon- and  $Z$ -exchanges have been evaluated by the authors of Refs. [18, 19] at the low energies ( $\sim 10$  MeV) relevant for the SNO experiment, which measured the neutrino flux from the  $^8\text{B}$  decay in the sun. These corrections are neglected in the present work, since its focus is on scattering of neutrinos with energies larger than 100 MeV. We are not (or not yet, at least) concerned with providing cross section calculations with % accuracy in this regime. Lastly, the nuclear response functions are defined as

$$R_{00}(q, \omega) = \frac{1}{3} \sum_M \sum_f \delta(\omega + m_d - E_f) \langle f | j^0(\mathbf{q}, \omega) | d, M \rangle \langle f | j^0(\mathbf{q}, \omega) | d, M \rangle^* , \quad (2.5)$$

$$R_{zz}(q, \omega) = \frac{1}{3} \sum_M \sum_f \delta(\omega + m_d - E_f) \langle f | j^z(\mathbf{q}, \omega) | d, M \rangle \langle f | j^z(\mathbf{q}, \omega) | d, M \rangle^* , \quad (2.6)$$

$$R_{0z}(q, \omega) = \frac{2}{3} \sum_M \sum_f \delta(\omega + m_d - E_f) \text{Re} \left[ \langle f | j^0(\mathbf{q}, \omega) | d, M \rangle \langle f | j^z(\mathbf{q}, \omega) | d, M \rangle^* \right] , \quad (2.7)$$

$$R_{xx+yy}(q, \omega) = \frac{1}{3} \sum_M \sum_f \delta(\omega + m_d - E_f) \left[ \langle f | j^x(\mathbf{q}, \omega) | d, M \rangle \langle f | j^x(\mathbf{q}, \omega) | d, M \rangle^* \right. \\ \left. + \langle f | j^y(\mathbf{q}, \omega) | d, M \rangle \langle f | j^y(\mathbf{q}, \omega) | d, M \rangle^* \right] , \quad (2.8)$$

$$R_{xy}(q, \omega) = \frac{2}{3} \sum_M \sum_f \delta(\omega + m_d - E_f) \text{Im} \left[ \langle f | j^x(\mathbf{q}, \omega) | d, M \rangle \langle f | j^y(\mathbf{q}, \omega) | d, M \rangle^* \right] , \quad (2.9)$$

where  $|d, M\rangle$  and  $|f\rangle$  represent, respectively, the initial deuteron state in spin projection  $M$  and the final two-nucleon state of energy  $E_f$ , and  $m_d$  is the deuteron rest mass. The three-momentum transfer  $\mathbf{q}$  is taken along the  $z$ -axis (i.e., the spin-quantization axis), and  $j^\mu(\mathbf{q}, \omega)$  is the time component (for  $\mu = 0$ ) or space component (for  $\mu = x, y, z$ ) of the NC or CC.

The expression above for the CC cross section is valid in the limit  $\epsilon' \simeq k'$ , in which the lepton rest mass is neglected. At small incident neutrino energy, this approximation is not correct. Inclusion of the lepton rest mass leads to changes in the kinematical factors multiplying the various response functions. The resulting cross section is given in Appendix A.

### III. NEUTRAL AND CHARGE-CHANGING WEAK CURRENTS

We denote the neutral and charge-changing weak currents as  $j_{NC}^\mu$  and  $j_{CC}^\mu$ , respectively. The former is given by

$$j_{NC}^\mu = -2 \sin^2 \theta_W j_{\gamma, S}^\mu + (1 - 2 \sin^2 \theta_W) j_{\gamma, z}^\mu + j_z^{\mu 5} , \quad (3.1)$$

where  $\theta_W$  is the Weinberg angle ( $\sin^2 \theta_W = 0.2312$  [17]),  $j_{\gamma, S}^\mu$  and  $j_{\gamma, z}^\mu$  denote, respectively, the isoscalar and isovector pieces of the electromagnetic current, and  $j_z^{\mu 5}$  denotes the isovector piece of the axial current (the  $z$  on the isovector terms indicates that they transform as the  $z$ -component of an isovector under rotations in isospin space). Isoscalar contributions to  $j_{NC}^\mu$  associated with strange quarks are ignored, since experiments at Bates [20] and JLab [21] have found them to be very small.

The charge-changing weak current is written as the sum of polar- and axial-vector components

$$j_{CC}^\mu = j_\pm^\mu + j_\pm^{\mu 5} , \quad j_\pm = j_x \pm i j_y . \quad (3.2)$$

The conserved-vector-current (CVC) constraint relates the polar-vector components  $j_b^\mu$  of the charge-changing weak current to the isovector component  $j_{\gamma, z}^\mu$  of the electromagnetic current via

$$[T_a, j_{\gamma, z}^\mu] = i \epsilon_{azb} j_b^\mu , \quad (3.3)$$

where  $T_a$  are isospin operators. We now turn to a discussion of the one- and two-body contributions to the NC and CC.

### A. One-body terms

The isoscalar components of the one-body electromagnetic current are given by

$$j_{\gamma,S}^0(i) = \left[ \frac{G_E^S(Q^2)}{2\sqrt{1+Q^2/(4m^2)}} - i \frac{2G_M^S(Q^2) - G_E^S(Q^2)}{8m^2} \mathbf{q} \cdot (\boldsymbol{\sigma}_i \times \mathbf{p}_i) \right] e^{i\mathbf{q} \cdot \mathbf{r}_i}, \quad (3.4)$$

$$\mathbf{j}_{\gamma,S}^\perp(i) = \left[ \frac{G_E^S(Q^2)}{2m} \mathbf{p}_i^\perp - i \frac{G_M^S(Q^2)}{4m} \mathbf{q} \times \boldsymbol{\sigma}_i \right] e^{i\mathbf{q} \cdot \mathbf{r}_i}, \quad (3.5)$$

$$j_{\gamma,S}^\parallel(i) = \frac{\omega}{q} j_{\gamma,S}^0(i), \quad (3.6)$$

and the corresponding isovector components of  $j_{\gamma,z}^\mu$  are obtained by the replacements

$$G_E^S(Q^2) \longrightarrow G_E^V(Q^2) \tau_{i,z}, \quad G_M^S(Q^2) \longrightarrow G_M^V(Q^2) \tau_{i,z}, \quad (3.7)$$

where  $G_E^{S/V}$  and  $G_M^{S/V}$  are the isoscalar/isovector combinations of the proton and neutron electric ( $E$ ) and magnetic ( $M$ ) form factors,  $\mathbf{r}_i$  and  $\mathbf{p}_i$  are the position and momentum operators of nucleon  $i$ ,  $\boldsymbol{\sigma}_i$  and  $\tau_{i,z}$  are its Pauli spin and isospin matrices, and  $m$  is the nucleon mass (0.9389 GeV). Note that we have decomposed  $\mathbf{j}_{\gamma,S}$  and  $\mathbf{j}_{\gamma,z}$  into transverse ( $\perp$ ) and longitudinal ( $\parallel$ ) components to the momentum transfer  $\mathbf{q}$ , and have used current conservation to relate the latter to the isoscalar and isovector charge operators  $j_{\gamma,S}^0$  and  $j_{\gamma,z}^0$ . The isovector components of the axial weak neutral current  $j_z^{\mu 5}$  are given by

$$j_z^{05}(i) = -\frac{G_A(Q^2)}{4m} \tau_{i,z} \boldsymbol{\sigma}_i \cdot [\mathbf{p}_i, e^{i\mathbf{q} \cdot \mathbf{r}_i}]_+, \quad (3.8)$$

$$\begin{aligned} \mathbf{j}_z^5(i) = & -\frac{G_A(Q^2)}{2} \tau_{i,z} \left[ \boldsymbol{\sigma}_i e^{i\mathbf{q} \cdot \mathbf{r}_i} - \frac{1}{4m^2} \left( \boldsymbol{\sigma}_i [\mathbf{p}_i^2, e^{i\mathbf{q} \cdot \mathbf{r}_i}]_+ - [(\boldsymbol{\sigma}_i \cdot \mathbf{p}_i) \mathbf{p}_i, e^{i\mathbf{q} \cdot \mathbf{r}_i}]_+ \right. \right. \\ & \left. \left. - \frac{1}{2} \boldsymbol{\sigma}_i \cdot \mathbf{q} [\mathbf{p}_i, e^{i\mathbf{q} \cdot \mathbf{r}_i}]_+ - \frac{1}{2} \mathbf{q} [\boldsymbol{\sigma}_i \cdot \mathbf{p}_i, e^{i\mathbf{q} \cdot \mathbf{r}_i}]_+ + i \mathbf{q} \times \mathbf{p}_i e^{i\mathbf{q} \cdot \mathbf{r}_i} \right) \right], \end{aligned} \quad (3.9)$$

where  $G_A$  is the nucleon axial form factor, and  $[\dots]_+$  denotes the anticommutator. The operators above include terms of order  $(v/c)^2$  in the non-relativistic expansion of the single-nucleon covariant currents. These have been neglected in the study of Ref. [12]. The proton and neutron electromagnetic and nucleon axial form factors are parametrized as

$$G_E^p(Q^2) = G_D(Q^2), \quad G_E^n(Q^2) = -\mu_n \frac{Q^2}{4m^2} \frac{G_D(Q^2)}{1+Q^2/m^2}, \quad (3.10)$$

$$G_M^p(Q^2) = \mu_p G_D(Q^2), \quad G_M^n(Q^2) = \mu_n G_D(Q^2), \quad (3.11)$$

$$G_D(Q^2) = \frac{1}{(1+Q^2/\Lambda^2)^2}, \quad G_A(Q^2) = \frac{g_A}{(1+Q^2/\Lambda_A^2)^2}, \quad (3.12)$$

from which the isoscalar and isovector combinations are obtained as  $G_{E,M}^{S/V} = G_{E,M}^p \pm G_{E,M}^n$ . The proton and neutron magnetic moments are  $\mu_p = 2.793$  and  $\mu_n = -1.913$  in units of nuclear magnetons (n.m.), and the nucleon axial-vector coupling constant is taken to be  $g_A = 1.2694$  [17]. The values for the cutoff masses  $\Lambda$  and  $\Lambda_A$  used in this work are 0.833 GeV and 1 GeV, respectively. The former is from fits to elastic electron scattering data off the proton and deuteron [22], while the latter is from an analysis of pion electroproduction [5] and neutrino scattering [6–8] data. Uncertainties in the  $Q^2$  dependence of the axial form factor, in particular the value of  $\Lambda_A$ , could significantly impact predictions for the neutrino cross sections under consideration. As mentioned earlier, recent analyses of neutrino quasi-elastic scattering data on nuclear targets [4] quote considerably larger values for  $\Lambda_A$ , in the range (1.20–1.35) GeV.

The polar-vector ( $j_\pm^\mu$ ) and axial-vector ( $j_\pm^{\mu 5}$ ) components of the charge-changing weak current are obtained, respectively, from  $j_{\gamma,z}^\mu$  and  $j_z^{\mu 5}$  by replacing

$$\tau_{i,z}/2 \longrightarrow \tau_{i,\pm} = (\tau_{i,x} \pm \tau_{i,y})/2. \quad (3.13)$$

However, in the case of  $j_{\pm}^{\mu 5}$ , in addition to the terms entering Eqs. (3.8)–(3.9), we also retain the induced pseudoscalar contribution, given by

$$j_{\pm}^{\mu 5}(i; PS) = -\frac{G_{PS}(Q^2)}{2m m_{\mu}} \tau_{i,\pm} q^{\mu} \boldsymbol{\sigma}_i \cdot \mathbf{q} e^{i\mathbf{q} \cdot \mathbf{r}_i} , \quad (3.14)$$

where the induced pseudoscalar form factor  $G_{PS}$  is parametrized as

$$G_{PS}(Q^2) = -\frac{2m_{\mu} m}{m_{\pi}^2 + Q^2} G_A(Q^2) . \quad (3.15)$$

This form factor is not well known [23]. The parameterization above is consistent with values extracted [24, 25] from precise measurements of muon-capture rates on hydrogen [26] and  $^3\text{He}$  [27], as well as with the most recent theoretical predictions based on chiral perturbation theory [28]. This contribution vanishes in NC-induced neutrino reactions.

## B. Two-body terms

Two-body terms in the neutral and charge-changing weak currents have been discussed in considerable detail in Refs. [29–31] (and references therein). We list the terms included in the present study—i.e., the subset of those derived in the above references expected to give the dominant two-body contributions to the processes of interest here—in the following two sub-sections for clarity of presentation and future reference in Sec. V. Unless stated otherwise, they are given in momentum space, and configuration-space expressions follow from

$$O(\mathbf{q}) = \int_{\mathbf{k}_i} \int_{\mathbf{K}_i} \int_{\mathbf{k}_j} \int_{\mathbf{K}_j} (2\pi)^3 \delta(\mathbf{k}_i + \mathbf{k}_j - \mathbf{q}) e^{i\mathbf{k}_i \cdot (\mathbf{r}'_i + \mathbf{r}_i)/2} e^{i\mathbf{K}_i \cdot (\mathbf{r}'_i - \mathbf{r}_i)} e^{i\mathbf{k}_j \cdot (\mathbf{r}'_j + \mathbf{r}_j)/2} e^{i\mathbf{K}_j \cdot (\mathbf{r}'_j - \mathbf{r}_j)} O(\mathbf{k}_i, \mathbf{K}_i, \mathbf{k}_j, \mathbf{K}_j) , \quad (3.16)$$

where  $\mathbf{k}_i = \mathbf{p}'_i - \mathbf{p}_i$  and  $\mathbf{K}_i = (\mathbf{p}'_i + \mathbf{p}_i)/2$ ,  $\mathbf{p}_i$  and  $\mathbf{p}'_i$  are the initial and final momenta of nucleon  $i$ , and

$$\int_{\mathbf{p}} \equiv \int \frac{d\mathbf{p}}{(2\pi)^3} . \quad (3.17)$$

These configuration-space operators are used in the calculations reported below.

### 1. Two-body vector terms

The two-body isovector current operator  $\mathbf{j}_{\gamma,z}(ij)$  consists of pseudoscalar- and vector-meson (referred to as  $\pi$ -like and  $\rho$ -like) exchange, and  $\Delta$ -excitation terms,

$$\mathbf{j}_{\gamma,z}(ij) = \sum_{c=\pi, \rho, \Delta} [\mathbf{j}_{\gamma,z}(ij; c) + i \rightleftharpoons j] . \quad (3.18)$$

The  $\pi$ -like and  $\rho$ -like exchange currents read:

$$\mathbf{j}_{\gamma,z}(ij; \pi) = i G_E^V(Q^2) (\boldsymbol{\tau}_i \times \boldsymbol{\tau}_j)_z v_{\pi}(k_j) \left[ \boldsymbol{\sigma}_i - \frac{\mathbf{k}_i - \mathbf{k}_j}{k_i^2 - k_j^2} (\boldsymbol{\sigma}_i \cdot \mathbf{k}_i) \right] \boldsymbol{\sigma}_j \cdot \mathbf{k}_j , \quad (3.19)$$

$$\begin{aligned} \mathbf{j}_{\gamma,z}(ij; \rho) = & -i G_E^V(Q^2) (\boldsymbol{\tau}_i \times \boldsymbol{\tau}_j)_z \left[ v_{\rho}(k_j) \boldsymbol{\sigma}_i \times (\boldsymbol{\sigma}_j \times \mathbf{k}_j) + \frac{v_{\rho}(k_j)}{k_i^2 - k_j^2} [(\mathbf{k}_i - \mathbf{k}_j)(\boldsymbol{\sigma}_i \times \mathbf{k}_i) \cdot (\boldsymbol{\sigma}_j \times \mathbf{k}_j) \right. \\ & \left. + (\boldsymbol{\sigma}_i \times \mathbf{k}_i) \boldsymbol{\sigma}_j \cdot (\mathbf{k}_i \times \mathbf{k}_j) + (\boldsymbol{\sigma}_j \times \mathbf{k}_j) \boldsymbol{\sigma}_i \cdot (\mathbf{k}_i \times \mathbf{k}_j) \right] - v_{\rho S}(k_j) \frac{\mathbf{k}_i - \mathbf{k}_j}{k_i^2 - k_j^2} , \end{aligned} \quad (3.20)$$

where

$$v_{\pi}(k) = v^{\sigma\tau}(k) - 2 v^{t\tau}(k) , \quad v_{\rho}(k) = v^{\sigma\tau}(k) + v^{t\tau}(k) , \quad v_{\rho S}(k) = v^{\tau}(k) , \quad (3.21)$$

and

$$v^\tau(k) = 4\pi \int_0^\infty r^2 dr j_0(kr) v^\tau(r) , \quad (3.22)$$

$$v^{\sigma\tau}(k) = \frac{4\pi}{k^2} \int_0^\infty r^2 dr [j_0(kr) - 1] v^{\sigma\tau}(r) , \quad (3.23)$$

$$v^{t\tau}(k) = \frac{4\pi}{k^2} \int_0^\infty r^2 dr j_2(kr) v^{t\tau}(r) . \quad (3.24)$$

Here  $v^\tau(r)$ ,  $v^{\sigma\tau}(r)$ ,  $v^{t\tau}(r)$  are the isospin-dependent central, spin-spin, and tensor components of the two-nucleon interaction (the AV18 in the present study), and  $j_l(kr)$  are spherical Bessel functions. The factor  $j_0(kr) - 1$  in the expression for  $v^{\sigma\tau}(k)$  ensures that its volume integral vanishes. In a one-boson-exchange (OBE) model, in which the isospin-dependent central, spin-spin, and tensor interactions are due to  $\pi$ - and  $\rho$ -meson exchange, the functions  $v_\pi(k)$ ,  $v_\rho(k)$ , and  $v_{\rho S}(k)$  simply reduce to

$$v_\pi(k) \longrightarrow -\frac{f_\pi^2}{m_\pi^2} \frac{h_\pi^2(k)}{k^2 + m_\pi^2} , \quad (3.25)$$

$$v_\rho(k) \longrightarrow -\frac{g_\rho^2 (1 + \kappa_\rho)^2}{4m^2} \frac{h_\rho^2(k)}{k^2 + m_\rho^2} , \quad (3.26)$$

$$v_{\rho S}(k) \longrightarrow g_\rho^2 \frac{h_\rho^2(k)}{k^2 + m_\rho^2} , \quad (3.27)$$

where  $m_\pi$  and  $m_\rho$  are the meson masses,  $f_\pi$ , and  $g_\rho$  and  $\kappa_\rho$  are the pseudovector  $\pi NN$ , and vector and tensor  $\rho NN$  coupling constants, and the hadronic form factors are parameterized as

$$h_\alpha(k) = \frac{\Lambda_\alpha^2 - m_\alpha^2}{\Lambda_\alpha^2 + k^2} , \quad \alpha = \pi, \rho . \quad (3.28)$$

While the AV18 interaction is not a OBE model, nevertheless the effective propagators  $v_\pi(k)$ ,  $v_\rho(k)$ , and  $v_{\rho S}(k)$  projected out of its  $v^\tau(k)$ ,  $v^{\sigma\tau}(k)$ , and  $v^{t\tau}(k)$  components are quite similar to those listed above with cutoff masses in the range (1.0–1.5) GeV. We note that the  $\pi$ -like and  $\rho$ -like currents with the  $v_\pi(k)$ ,  $v_\rho(k)$ , and  $v_{\rho S}(k)$  defined in Eq. (3.21) satisfy by construction the current conservation relation with the AV18  $\tau$ ,  $\sigma\tau$ , and  $t\tau$  interaction components (for a discussion of the issue of current conservation in relation to the momentum-dependent terms of the AV18, see Ref. [31]).

The isovector  $\Delta$ -excitation current is written in configuration space as (for a derivation based on a perturbative treatment of  $\Delta$ -isobar degrees of freedom in nuclear wave functions, see Ref. [29])

$$\mathbf{j}_{\gamma,z}(ij; \Delta) = -i \frac{G_{\gamma N \Delta}(Q^2)}{2m(m - m_\Delta)} e^{i\mathbf{q} \cdot \mathbf{r}_i} \left[ v_{\Delta N}^\dagger(ij) \mathbf{q} \times \mathbf{S}_i T_{i,z} + \text{adjoint} \right] , \quad (3.29)$$

where  $\mathbf{S}$  and  $\mathbf{T}$  are spin- and isospin-transition operators converting a nucleon into a  $\Delta$  isobar and satisfying the identity

$$\mathbf{S}^\dagger \cdot \mathbf{A} \mathbf{S} \cdot \mathbf{B} = \frac{2}{3} \mathbf{A} \cdot \mathbf{B} - \frac{i}{3} \boldsymbol{\sigma} \cdot (\mathbf{A} \times \mathbf{B}) , \quad (3.30)$$

$v_{\Delta N}(ij)$  is the  $NN$  to  $\Delta N$  transition potential,

$$v_{\Delta N}(ij) = \left[ v_{\Delta N}^{\sigma\tau}(r_{ij}) \mathbf{S}_i \cdot \boldsymbol{\sigma}_j + v_{\Delta N}^{t\tau}(r_{ij}) S_{ij}^{\Delta N} \right] \mathbf{T}_i \cdot \boldsymbol{\tau}_j , \quad (3.31)$$

$S_{ij}^{\Delta N}$  is the tensor operator obtained by replacing  $\boldsymbol{\sigma}_i$  with  $\mathbf{S}_i$ , the regularized spin-spin and tensor radial functions  $v_{\Delta N}^{\sigma\tau}(r)$  and  $v_{\Delta N}^{t\tau}(r)$  are defined as

$$v_{\Delta N}^{\sigma\tau}(r) = \frac{f_\pi f_\pi^*}{4\pi} \frac{m_\pi}{3} \frac{e^{-x}}{x} \left( 1 - e^{-\lambda x^2} \right) , \quad (3.32)$$

$$v_{\Delta N}^{t\tau}(r) = \frac{f_\pi f_\pi^*}{4\pi} \frac{m_\pi}{3} \left( 1 + \frac{3}{x} + \frac{3}{x^2} \right) \frac{e^{-x}}{x} \left( 1 - e^{-\lambda x^2} \right)^2 , \quad (3.33)$$

and  $x = m_\pi r$ ,  $f_\pi^*$  is the  $\pi N\Delta$  coupling constant ( $f_\pi^* = 2.19 f_\pi$  from the width of the  $\Delta$ ), and the parameter in the short-range cutoff function is taken as  $\lambda = 4.29$  (from the AV18). Finally, the  $\gamma N\Delta$  electromagnetic transition form factor  $G_{\gamma N\Delta}$  is parameterized as

$$G_{\gamma N\Delta}(Q^2) = \frac{\mu_{\gamma N\Delta}}{(1 + Q^2/\Lambda_{\Delta,1}^2)^2 \sqrt{1 + Q^2/\Lambda_{\Delta,2}^2}} , \quad (3.34)$$

where the transition magnetic moment  $\mu_{\gamma N\Delta}$  is 3 n.m., as obtained in an analysis of  $\gamma N$  data in the  $\Delta$ -resonance region [32]. This analysis also gives  $\Lambda_{\Delta,1}=0.84$  GeV and  $\Lambda_{\Delta,2}=1.2$  GeV.

The two-body isoscalar current operator  $\mathbf{j}_{\gamma,S}(ij)$  considered in the present study only includes the contribution associated with the  $\rho\pi\gamma$  transition mechanism,

$$\mathbf{j}_{\gamma,S}(ij) = \mathbf{j}_{\gamma,S}(ij; \rho\pi) + i \rightleftharpoons j , \quad (3.35)$$

where

$$\mathbf{j}_{\gamma,S}(ij; \rho\pi) = -i G_{\rho\pi\gamma}(Q^2) g_{\rho\pi\gamma} \frac{f_\pi}{m_\pi} \frac{g_\rho}{m_\rho} \boldsymbol{\tau}_i \cdot \boldsymbol{\tau}_j \frac{h_\rho(k_i)}{k_i^2 + m_\rho^2} \frac{h_\pi(k_j)}{k_j^2 + m_\pi^2} (\mathbf{k}_i \times \mathbf{k}_j) \boldsymbol{\sigma}_j \cdot \mathbf{k}_j , \quad (3.36)$$

The combination of coupling constants  $g_{\rho\pi\gamma} f_\pi g_\rho$  is taken as 1.37, and the cutoff masses  $\Lambda_\pi$  and  $\Lambda_\rho$  as 0.75 GeV and 1.25 GeV, respectively, from a study of the deuteron magnetic form factor [33]. The  $Q^2$  dependence of the electromagnetic transition form factor  $G_{\rho\pi\gamma}(Q^2)$  is modeled by using vector-meson dominance,

$$G_{\rho\pi\gamma}(Q^2) = \frac{1}{1 + Q^2/m_\omega^2} , \quad (3.37)$$

where  $m_\omega$  is the  $\omega$ -meson mass.

The two-body isovector and isoscalar electromagnetic charge operators  $j_{\gamma,z}^0$  and  $j_{\gamma,S}^0$  consist of terms associated with  $\pi$ -like and  $\rho$ -like exchanges

$$j_{\gamma,z/S}^0(ij) = \sum_{c=\pi,\rho} \left[ j_{\gamma,z/S}^0(ij; c) + i \rightleftharpoons j \right] , \quad (3.38)$$

where

$$j_{\gamma,z}^0(ij; \pi) = \frac{F_1^V(Q^2)}{2m} \tau_{z,j} v_\pi(k_j) (\boldsymbol{\sigma}_i \cdot \mathbf{q}) (\boldsymbol{\sigma}_j \cdot \mathbf{k}_j) , \quad (3.39)$$

$$j_{\gamma,z}^0(ij; \rho) = \frac{F_1^V(Q^2)}{2m} \tau_{z,j} v_\rho(k_j) (\boldsymbol{\sigma}_i \times \mathbf{q}) \cdot (\boldsymbol{\sigma}_j \times \mathbf{k}_j) , \quad (3.40)$$

and

$$j_{\gamma,S}^0(ij; \pi) = \frac{F_1^S(Q^2)}{2m} \boldsymbol{\tau}_i \cdot \boldsymbol{\tau}_j v_\pi(k_j) (\boldsymbol{\sigma}_i \cdot \mathbf{q}) (\boldsymbol{\sigma}_j \cdot \mathbf{k}_j) , \quad (3.41)$$

$$j_{\gamma,S}^0(ij; \rho) = \frac{F_1^S(Q^2)}{2m} \boldsymbol{\tau}_i \cdot \boldsymbol{\tau}_j v_\rho(k_j) (\boldsymbol{\sigma}_i \times \mathbf{q}) \cdot (\boldsymbol{\sigma}_j \times \mathbf{k}_j) , \quad (3.42)$$

with  $v_\pi(k)$  and  $v_\rho(k)$  as defined in Eqs. (3.21). The nucleon electromagnetic Dirac and Pauli form factors  $F_1^{S/V}$  and  $F_2^{S/V}$  are obtained from

$$F_1^{S/V}(Q^2) = \frac{G_E^{S/V}(Q^2) + \eta G_M^{S/V}(Q^2)}{1 + \eta} , \quad (3.43)$$

$$F_2^{S/V}(Q^2) = \frac{G_M^{S/V}(Q^2) - G_E^{S/V}(Q^2)}{1 + \eta} , \quad (3.44)$$

with  $\eta = Q^2/(4m^2)$ .

The polar-vector components  $j_\pm^\mu$  of the charge-changing weak current  $j_{CC}^\mu$  are obtained from  $j_{\gamma,z}^\mu$  via CVC, which implies the replacements

$$(\boldsymbol{\tau}_i \times \boldsymbol{\tau}_j)_z \longrightarrow (\boldsymbol{\tau}_i \times \boldsymbol{\tau}_j)_\pm = (\boldsymbol{\tau}_i \times \boldsymbol{\tau}_j)_x \pm i (\boldsymbol{\tau}_i \times \boldsymbol{\tau}_j)_y \quad (3.45)$$

in Eqs. (3.19)–(3.20),

$$T_{i,z}/2 \longrightarrow T_{i,\pm} = (T_{i,x} \pm i T_{i,y})/2 \quad (3.46)$$

in Eq. (3.29), and the replacement (3.13) in Eqs. (3.39)–(3.40). Only the transverse components (perpendicular to  $\mathbf{q}$ ) of the vector part of the NC and CC are explicitly included in the calculations to follow. Their longitudinal components have already been effectively accounted for by the replacement in Eq. (3.6) (and the similar one for the isovector terms). Lastly, we note that in the study of Ref. [12] the  $\rho$ -meson exchange and  $\rho\pi$  transition contributions to the two-body vector current, and  $\pi$ - and  $\rho$ -exchange contributions to the two-body vector charge have been neglected. Furthermore, the  $\pi$ -exchange and  $\Delta$  excitation currents are regularized by introducing a monopole form factor ( $\Lambda_\pi = 4.8 \text{ fm}^{-1}$ ), which naturally leads to a different short-range behavior of these currents than obtained here.

## 2. Two-body axial terms

TABLE I: Contributions to the GT matrix element in tritium  $\beta$ -decay. The one-body (1-b) NR and RC contributions are, respectively, from the leading and  $1/m^2$  terms in Eq. (3.9); the two-body (2-b) contributions are from Eqs. (3.48)–(3.51). Set I (II) corresponds to the cutoff choices  $\Lambda_\pi = \Lambda_\rho = 1.2 \text{ GeV}$  ( $\Lambda_\pi = 1.72 \text{ GeV}$  and  $\Lambda_\rho = 1.31 \text{ GeV}$ ). The  $N$  to  $\Delta$  axial coupling constant  $g_A^*$  for each set is obtained by fitting the experimental value of the GT matrix element, given by  $0.955 \pm 0.002$  [25].

	Set I	Set II
1-b (NR)	+0.9213	+0.9213
1-b (RC)	−0.0085	−0.0085
2-b ( $\pi$ )	+0.0078	+0.0123
2-b ( $\rho$ )	−0.0042	−0.0055
2-b ( $\rho\pi$ )	+0.0123	+0.0196
2-b ( $\Delta$ )	+0.0263	+0.0159
$g_A^*/g_A$	0.614	0.371

The axial parts of the neutral and charge-changing weak current operators consist of contributions associated with  $\pi$ - and  $\rho$ -meson exchanges, the axial  $\rho\pi$  transition mechanism, and a  $\Delta$  excitation term

$$\mathbf{j}_a^5(ij) = \sum_{c=\pi, \rho, \rho\pi, \Delta} [\mathbf{j}_a^5(ij; c) + i \equiv j] , \quad (3.47)$$

where the isospin component  $a$  is either  $z$  for NC or  $\pm$  for CC. The  $\pi$ - and  $\rho$ -meson exchange and  $\rho\pi$  transition axial currents read, respectively,

$$\mathbf{j}_z^5(ij; \pi) = \frac{G_A(Q^2)}{2m} \frac{f_\pi^2}{m_\pi^2} \frac{h_\pi^2(k_j)}{k_j^2 + m_\pi^2} \left[ (\boldsymbol{\tau}_i \times \boldsymbol{\tau}_j)_z \boldsymbol{\sigma}_i \times \mathbf{k}_j - \tau_{j,z} (\mathbf{q} + 2i \boldsymbol{\sigma}_i \times \mathbf{K}_i) \right] \boldsymbol{\sigma}_j \cdot \mathbf{k}_j , \quad (3.48)$$

$$\begin{aligned} \mathbf{j}_z^5(ij; \rho) = & -\frac{G_A(Q^2)}{2m} \frac{g_\rho^2 (1+k_\rho)^2}{4m^2} \frac{h_\rho^2(k_j)}{k_j^2 + m_\rho^2} \left[ (\boldsymbol{\tau}_i \times \boldsymbol{\tau}_j)_z \left[ \mathbf{q} \boldsymbol{\sigma}_i \cdot (\boldsymbol{\sigma}_j \times \mathbf{k}_j) + 2i (\boldsymbol{\sigma}_j \times \mathbf{k}_j) \times \mathbf{K}_i \right. \right. \\ & \left. \left. - [\boldsymbol{\sigma}_i \times (\boldsymbol{\sigma}_j \times \mathbf{k}_j)] \times \mathbf{k}_j \right] + \tau_{j,z} \left[ (\boldsymbol{\sigma}_j \times \mathbf{k}_j) \times \mathbf{k}_j - 2i [\boldsymbol{\sigma}_i \times (\boldsymbol{\sigma}_j \times \mathbf{k}_j)] \times \mathbf{K}_i \right] \right] , \end{aligned} \quad (3.49)$$

$$\mathbf{j}_z^5(ij; \rho\pi) = -\frac{G_A(Q^2)}{m} g_\rho^2 \frac{h_\rho(k_i)}{k_i^2 + m_\rho^2} \frac{h_\pi(k_j)}{k_j^2 + m_\pi^2} (\boldsymbol{\tau}_i \times \boldsymbol{\tau}_j)_z \left[ (1 + \kappa_\rho) \boldsymbol{\sigma}_i \times \mathbf{k}_i - 2i \mathbf{K}_i \right] \boldsymbol{\sigma}_j \cdot \mathbf{k}_j , \quad (3.50)$$

while the  $\Delta$  excitation axial current is obtained from [29]

$$\mathbf{j}_z^5(ij; \Delta) = -\frac{G_A^*(Q^2)}{2(m - m_\Delta)} e^{i\mathbf{q} \cdot \mathbf{r}_i} \left[ v_{\Delta N}^\dagger(ij) \mathbf{S}_i T_{i,z} + \text{adjoint} \right] , \quad (3.51)$$

where the (unknown)  $N$  to  $\Delta$  axial form factor is parameterized as

$$G_A^*(Q^2) = \frac{g_A^*}{(1 + Q^2/\Lambda_A^2)^2} . \quad (3.52)$$



The charge-changing axial currents follow by replacing the isospin operators as in Eqs. (3.13) and (3.45)–(3.46). The values for the  $\pi$ - and  $\rho$ -meson coupling constants are taken from the CD-Bonn one-boson-exchange model [34],  $f_\pi^2/(4\pi) = 0.075$ ,  $g_\rho^2/(4\pi) = 0.84$ , and  $\kappa_\rho = 6.1$ , while two different sets of cutoff masses  $\Lambda_\pi$  and  $\Lambda_\rho$  are used in the present work:  $\Lambda_\pi = \Lambda_\rho = 1.2$  GeV (Set I) in line with the cutoff masses extracted from the  $\pi$ -like and  $\rho$ -like exchanges associated with the AV18 model;  $\Lambda_\pi = 1.72$  GeV and  $\Lambda_\rho = 1.31$  GeV (Set II) from the CD-Bonn model. In the  $N$  to  $\Delta$  axial current, the  $Q^2$  dependence of the form factor is taken to be the same as that of the nucleon; however, the value for the transition axial coupling constant  $g_A^*$  is determined by fitting the Gamow-Teller (GT) matrix element of tritium  $\beta$ -decay [25] in a calculation based on trinucleon wave functions corresponding to the AV18/UIX Hamiltonian and the present model for the axial current. The values corresponding to Set I and II of cutoff masses are listed in Table I.

Finally, in the present study the axial charge operator is taken to include only the pion-exchange term, whose structure and strength are determined by soft-pion theorem and current algebra arguments [35]

$$j_a^{05}(ij) = j_a^{05}(ij; \pi) + i \equiv j, \quad (3.53)$$

where

$$j_a^{05}(ij; \pi) = -i \frac{G_A(Q^2)}{4F_\pi^2} \frac{h_\pi^2(k_i)}{k_i^2 + m_\pi^2} (\boldsymbol{\tau}_i \times \boldsymbol{\tau}_j)_a \boldsymbol{\sigma}_i \cdot \mathbf{k}_i, \quad (3.54)$$

$F_\pi$  is pion decay amplitude ( $F_\pi = 93$  MeV), and the  $Q^2$  dependence of the associated form factor is assumed to be the same as in the nucleon. We conclude by noting that the model described above for the two-body axial charge and current operators is essentially the same of that used in Ref. [12], apart from differences in the values of the cutoff masses for the hadronic form factors of the meson exchange terms, and a different treatment of the  $\Delta$  excitation current. However, it is important to stress that both here and in Ref. [12] the two-body axial currents are constrained to reproduce the experimental tritium  $\beta$ -decay rate.

#### IV. CALCULATION

The two-body scattering- and bound-state problems are solved in momentum space with the methods discussed in Ref. [36], which facilitates calculations with a non-local potential such as CD Bonn. We briefly summarize them in the next two sub-sections for clarity. In the last sub-section we discuss the calculation of the weak current matrix elements, response functions, and cross sections.

##### A. The scattering-state problem in momentum space

In the case of scattering (setting aside the treatment of the Coulomb interaction for the time being), we solve for the  $K$ -matrix in channel  $JST$  (hereafter,  $L$  is the relative orbital angular momentum,  $S$  and  $T$  are the total spin and isospin, and  $J$  is the total angular momentum, and  $(-1)^{L+S+T} = -1$ )

$$K_{L'L}^{JST}(p'; p) = v_{L'L}^{JST}(p'; p) + \frac{4\mu}{\pi} \int_0^\infty dk k^2 \sum_{L''} v_{L'L''}^{JST}(p'; k) \frac{\mathcal{P}}{p^2 - k^2} K_{L''L}^{JST}(k; p), \quad (4.1)$$

where  $\mu$  is the two-nucleon reduced mass,  $\mathcal{P}$  denotes a principal-value integration, and  $v_{L'L}^{JST}(p', p)$  are the  $p$ -space matrix elements of the potential, projected in channel  $JST$  [36]. We should note the presence of the somewhat unconventional phase factor  $i^{L-L'}$  included in the matrix elements  $v_{L'L}^{JST}(p'; p)$  [36], which makes the states used here differ by a factor  $i^L$  from those usually adopted in nucleon-nucleon scattering analyses. The integral equations (4.1) are discretized, and the resulting systems of linear equations are solved by direct numerical inversion. The principal-value integration is eliminated by a standard subtraction technique [37]. Phase shifts in channel  $JST$  are easily obtained from the on-shell  $S$ -matrix related to the (on-shell)  $K$ -matrix by

$$S^{JST}(p) = [1 + 2i\mu p K^{JST}(p; p)]^{-1} [1 - 2i\mu p K^{JST}(p; p)], \quad (4.2)$$

while  $r$ -space wave functions follow from

$$z_{L'L}^{JST}(r; p) = \left[ j(pr) + \frac{4\mu}{\pi} \int_0^\infty dk k^2 j(kr) \frac{\mathcal{P}}{p^2 - k^2} K^{JST}(k; p) \right]_{L'L''} \left[ 1 + 2i\mu p K^{JST}(p; p) \right]_{L''L}^{-1}, \quad (4.3)$$

where the matrix  $[j(pr)]_{L'L} \equiv \delta_{L'L} j_L(pr)$  has been introduced for convenience. The (complex) radial wave functions  $z_{L'L}^{JST}(r)$  behave in the asymptotic region  $r \rightarrow \infty$  as

$$z_{L'L}^{JST}(r; p) \simeq \frac{1}{2} \left[ \delta_{L'L} h_L^{(2)}(pr) + h_{L'}^{(1)}(pr) S_{L'L}^{JST}(p) \right], \quad (4.4)$$

where the functions  $h_L^{(1,2)}(pr)$  are defined in terms of the regular and irregular ( $n_L$ ) spherical Bessel functions as

$$h_L^{(1,2)}(y) = j_L(y) \pm i n_L(y). \quad (4.5)$$

In the calculation of the response functions that follows, scattering wave functions with incoming-wave boundary condition  $(-)$  are required. These are written as

$$\begin{aligned} \psi_{SM_S, TM_T}^{(-)}(\mathbf{r}; \mathbf{p}) = & 4\pi\sqrt{2} \sum_{JM_J, J \leq J_{\max}} \sum_{LL'} i^{L'} Z_{LSM_S}^{JM_J*}(\hat{\mathbf{p}}) \left[ z_{L'L}^{JST*}(r; p) - \delta_{L'L} j_L(pr) \right] \mathcal{Y}_{L'SJ}^{M_J}(\hat{\mathbf{r}}) \eta_{MT}^T \\ & + \frac{1}{\sqrt{2}} \left[ e^{i\mathbf{p} \cdot \mathbf{r}} - (-)^{S+T} e^{-i\mathbf{p} \cdot \mathbf{r}} \right] \chi_{MS}^S \eta_{MT}^T, \end{aligned} \quad (4.6)$$

where  $\chi_{MS}^S$  and  $\eta_{MT}^T$  are two-nucleon spin and isospin states, respectively,  $\mathcal{Y}_{L'SJ}^{M_J}$  are standard spin-angle functions,

$$Z_{LSM_S}^{JM_J}(\hat{\mathbf{p}}) \equiv \sum_{M_L} \langle LM_L, SM_S | JM_J \rangle Y_{LM_L}(\hat{\mathbf{p}}), \quad (4.7)$$

and  $\langle LM_L, SM_S | JM_J \rangle$  are Clebsch-Gordan coefficients. Note that the wave function in Eq. (4.6) retains interaction effects only in channels with  $J \leq J_{\max}$ , and reduces to plane waves for  $J > J_{\max}$ .

When the Coulomb interaction is present, we use the method developed originally in Ref. [38], which allows us to solve the  $pp$  scattering problem in momentum space [39]. It consists essentially in separating the potential into short- and long-range parts  $v_S$  and  $v_L$ , where  $v_L$  only includes the Coulomb potential  $v_C$  and  $v_S$  includes, in addition to  $v_C$ , the nuclear potential  $v$ . Then the standard momentum-space technique outlined earlier can be used to solve the problem with  $v_S$ , and the corresponding radial wave functions behave as

$$z_{S;L'L}^{JS1}(r; p) \simeq \frac{a_L}{2} \left[ \delta_{L'L} h_L^{(2)}(pr) + h_{L'}^{(1)}(pr) S_{S;L'L}^{JS1}(p) \right], \quad (4.8)$$

where  $S_S^{JS1}$  is the  $S$ -matrix in this case (with  $T = 1$ ), and the  $a_L$  are normalization constants. The wave functions  $z_{S;L'L}^{JS1}$  should match smoothly those relative to  $v_S + v_L$ , which behave asymptotically as

$$z_{L'L}^{JS1}(r; p) \simeq \frac{1}{2} \left[ \delta_{L'L} \bar{h}_L^{(2)}(\xi, pr) + \bar{h}_{L'}^{(1)}(\xi, pr) S_{L'L}^{JS1}(p) \right], \quad (4.9)$$

where

$$\bar{h}_L^{(1,2)}(\xi, y) = [F_L(\xi; y) \mp G_L(\xi; y)] / y, \quad \xi = \alpha \mu / p, \quad (4.10)$$

and  $F_L$  and  $G_L$  are the regular and irregular Coulomb functions. Carrying out the matching for the functions and their first derivatives leads to a relation between  $S_S^{JS1}$  and  $S^{JS1}$  and a determination of the normalization constants [39]. Finally,  $pp$  scattering wave functions with incoming-wave boundary conditions are written as in Eq. (4.6) with  $T, M_T = 1, 1$  and the replacement

$$z_{L'L}^{JS1*}(r; p) \longrightarrow e^{-i\sigma_L} z_{L'L}^{JS1*}(r; p), \quad (4.11)$$

where  $\sigma_L$  is the Coulomb phase shift,

$$\sigma_L = \arg [\Gamma(L + 1 + i\xi)]. \quad (4.12)$$

Hence, Coulomb interaction effects are retained only in channels with  $J \leq J_{\max}$ , and are ignored in those with  $J > J_{\max}$ .

### B. The bound-state problem in momentum space

The deuteron wave function is written in  $r$ -space as

$$\psi_M(\mathbf{r}) = \sum_{L=0,2} i^L u_L(r) \mathcal{Y}_{L11}^M(\hat{\mathbf{r}}) \eta_0^0, \quad (4.13)$$

and the radial wave functions  $u_L(r)$  ( $L = 0, 2$ ) follow from

$$u_L(r) = \frac{2}{\pi} \int_0^\infty dp p^2 j_L(pr) \bar{u}_L(p). \quad (4.14)$$

The  $p$ -space wave functions  $\bar{u}_L(p)$  are obtained from solution of the homogeneous integral equations

$$\bar{u}_L(p) = \frac{1}{E_d - p^2/(2\mu)} \frac{2}{\pi} \int_0^\infty dk k^2 \sum_{L'=0,2} v_{LL'}^{110}(p; k) \bar{u}_{L'}(k). \quad (4.15)$$

Here,  $v_{L'L}^{110}$  is the nuclear potential in the  $JST = 110$  channel, and  $E_d$  is the deuteron energy ( $E_d = -2.225$  MeV). We again note the unconventional phase  $i^L$  in Eq. (4.13).

### C. Matrix elements, response functions, and cross sections

The deuteron wave function in Eq. (4.13) is written, for each spatial configuration  $\mathbf{r}$ , as a vector in the spin-isospin space of the two nucleons,

$$\psi_M(\mathbf{r}) = \sum_{n=1}^8 \psi_M^{(n)}(\mathbf{r}) |n\rangle, \quad (4.16)$$

where  $|n\rangle = (p \uparrow)_1 (n \uparrow)_2, (n \uparrow)_1 (p \uparrow)_2, \dots, (n \downarrow)_1 (p \downarrow)_2$  and  $\psi_M^{(n)}$  are the components of  $\psi_M$  in this basis. In the NC-induced processes, the scattering wave function in Eq. (4.6) is expanded on the same basis; however, in the CC-induced processes the  $pp$  or  $nn$  scattering wave functions are expanded on the (spin only) basis  $|m\rangle = \uparrow\uparrow, \downarrow\uparrow, \uparrow\downarrow$ , and  $\downarrow\downarrow$  for  $pp$  or  $nn$ . Matrix elements of the weak current operators are written schematically as

$$\langle f | O | d, M \rangle = \int d\mathbf{r} \sum_{n', n} \psi_f^{(n')*}(\mathbf{r}) O_{n', n}(\mathbf{r}) \psi_M^{(n)}(\mathbf{r}), \quad (4.17)$$

where the momentum- and energy-transfer dependence is understood. The spin-isospin algebra is performed exactly with techniques similar to those developed in Ref. [42], while the  $\mathbf{r}$ -space integrations are carried out efficiently by Gaussian quadratures. Note that no multipole expansion of the transition operators is required. When momentum operators are present, they are taken to act on the right (deuteron) wave function. For example, the one-body axial charge operator is written as

$$O(\mathbf{r}) \psi_M(\mathbf{r}) \longrightarrow -\frac{G_A(Q^2)}{4m} \left[ e^{i\mathbf{q}\cdot\mathbf{r}/2} \boldsymbol{\sigma}_1 \cdot (-2i\boldsymbol{\nabla} + \mathbf{q}) \tau_{1,z} + 1 \right] \psi_M(\mathbf{r}), \quad (4.18)$$

and the derivatives are evaluated numerically as

$$\nabla_\alpha \psi_M(\mathbf{r}) \simeq \frac{\psi_M(\mathbf{r} + \delta \hat{\mathbf{e}}_\alpha) - \psi_M(\mathbf{r} - \delta \hat{\mathbf{e}}_\alpha)}{2\delta}, \quad (4.19)$$

where  $\hat{\mathbf{e}}_\alpha$  is a unit vector in the  $\alpha$ -direction, and  $\delta$  is a small increment. Once the matrix elements have been computed, response functions are evaluated (in the lab frame) via

$$R_{ab}(q, \omega) = \frac{1}{3} \sum_M \sum_{SM_S, T} \int \frac{d\mathbf{p}}{(2\pi)^3} \frac{1}{2} \delta(\omega + m_d - E_+ - E_-) f_{ab}^{SM_S, TM_T; M}(\mathbf{q}, \mathbf{p}), \quad (4.20)$$

with

$$f_{ab}^{SM_S, TM_T; M}(\mathbf{q}, \mathbf{p}) = \langle \mathbf{q}, \mathbf{p}; SM_S, TM_T | O_a(\mathbf{q}, \omega) | d, M \rangle \langle \mathbf{q}, \mathbf{p}; SM_S, TM_T | O_b(\mathbf{q}, \omega) | d, M \rangle^*, \quad (4.21)$$

where  $|\mathbf{q}, \mathbf{p}; SM_S, TM_T\rangle$  represents the final two-nucleon scattering state with total momentum  $\mathbf{q}$  and relative momentum  $\mathbf{p}$ ,  $m_d$  is the deuteron rest mass, and  $E_{\pm}$  are the nucleons' energies in the final state,

$$E_{\pm} = \sqrt{(\mathbf{q}/2 \pm \mathbf{p})^2 + m^2} . \quad (4.22)$$

The factor  $1/2$  in Eq. (4.20) is to avoid double-counting the contribution of the final states (which are antisymmetrized), and the pair isospin  $T$  assumes the values  $T = 0, 1$  with  $M_T = 0$  for NC processes, and  $T = 1$  with  $M_T = 1$  or  $-1$  for CC processes. The  $\delta$ -function is integrated out, and

$$R_{ab}(q, \omega) = \frac{1}{24\pi^2} \sum_M \sum_{SM_S, T} \int_{-1}^{+1} dx p^2 \left| \frac{p+xq/2}{E_+} + \frac{p-xq/2}{E_-} \right|^{-1} f_{ab}^{SM_S, TM_T; M}(q, p, x) , \quad (4.23)$$

where  $x = \hat{\mathbf{q}} \cdot \hat{\mathbf{p}}$ , and the magnitude  $p$  of the relative momentum is fixed by energy conservation. This magnitude depends on  $q$ ,  $\omega$ , and  $x$ . However, in order to reduce the computational effort, the scattering states entering the product of matrix elements  $f_{ab}$  are obtained at the energy

$$4(\bar{p}^2 + m^2) = (\omega + m_d)^2 - q^2 , \quad (4.24)$$

which only depends on  $q$  and  $\omega$ . Lastly, Gauss points ( $\sim 50$ ) are used to perform the  $x$ -integration accurately. Extensive and independent tests of the computer programs have been completed successfully.

Total cross sections are obtained by direct integration of Eq. (2.3) by evaluating the differential cross sections on a grid of Gauss points in  $\epsilon'$  (the lepton final energy) and  $\theta$  (its scattering angle). There are kinematical constraints on the allowed values for  $\epsilon'$  and  $\theta$ , which follow from the requirement  $\bar{p}^2 \geq 0$ :

$$\epsilon \sqrt{\epsilon'^2 - m_l^2} \cos \theta \geq (\epsilon + m_d)(\epsilon' - \bar{\epsilon}) , \quad \bar{\epsilon} = \frac{m_d(\epsilon - \epsilon_{\text{th}}) + m_l(m_l + 2m)}{\epsilon + m_d} , \quad (4.25)$$

where  $\epsilon_{\text{th}}$  is the threshold energy for the initial neutrino ( $\epsilon > \epsilon_{\text{th}}$ ),

$$\epsilon_{\text{th}} = \frac{(m_l + 2m)^2 - m_d^2}{2m_d} , \quad (4.26)$$

$m_l$  is the rest mass of the final lepton ( $m_l = 0$  in the NC case), and  $m = (m_p + m_n)/2$  for NC reactions or  $m = m_p$  ( $m_n$ ) for charge-raising (charge-lowering) reactions. These kinematical constraints imply:

$$m_l \leq \epsilon' \leq \epsilon'_- \quad \text{for} \quad -1 \leq \cos \theta \leq 0 , \quad (4.27)$$

$$m_l \leq \epsilon' \leq \epsilon'_+ \quad \text{for} \quad 0 \leq \cos \theta \leq 1 , \quad (4.28)$$

where the limits  $\epsilon'_{\pm}$  are defined as

$$\epsilon'_{\pm} = \frac{\bar{\epsilon} \pm \sqrt{\bar{\epsilon}^2 - (1 - \beta^2 \cos^2 \theta)(\bar{\epsilon}^2 + m_l^2 \beta^2 \cos^2 \theta)}}{1 - \beta^2 \cos^2 \theta} , \quad \beta = \frac{1}{1 + m_d/\epsilon} . \quad (4.29)$$

In the case of NC reactions ( $m_l = 0$ ), they are simply given by

$$0 \leq \epsilon' \leq \frac{\bar{\epsilon}}{1 - \beta \cos \theta} \quad \text{for} \quad -1 \leq \cos \theta \leq 1 . \quad (4.30)$$

## V. RESULTS

Cross section values obtained with the AV18 interaction and the one- and two-body terms in the electroweak current discussed in Sec. III are listed in Tables II–IV for initial neutrino energies in the range (5–1000) MeV. The two-body axial currents are those corresponding to Set I in Table I. The two-nucleon ( $NN$ ) scattering states are written as in Eq. (4.6): they include interaction effects in channels with  $J \leq J_{\text{max}} = 5$  and reduce to spherical Bessel functions (i.e., plane waves) for  $J > J_{\text{max}}$ . The relative kinetic energy  $T = 2(\bar{p}^2 + m^2)^{1/2} - 2m$ , where  $\bar{p}$  is defined in Eq. (4.24), changes over a wide range as the initial neutrino energy increases up to 1 GeV and the final lepton energy and scattering angle vary over the allowed kinematical regions: at  $\epsilon = 50$  MeV,  $0 \lesssim T \lesssim 48$  MeV; at  $\epsilon = 500$  MeV,  $0 \lesssim T \lesssim 445$  MeV; and at  $\epsilon = 1000$  MeV,  $0 \lesssim T \lesssim 819$  MeV. These relative energies (at the larger values of

TABLE II: Total cross sections in  $\text{cm}^2$  for the NC- and CC-induced processes on the deuteron as function of the initial neutrino energy  $\epsilon$ , obtained with the AV18 potential and the inclusion of one- and two-body terms in the weak current. The number in parentheses, “ $-x$ ”, denotes  $10^{-x}$ ; for instance an entry like 9.561(−44) stands for  $9.561 \times 10^{-44} \text{ cm}^2$ .

$\epsilon$ (MeV)	$\nu_l$ -NC	$\bar{\nu}_l$ -NC	$\nu_e$ -CC	$\bar{\nu}_e$ -CC
5	9.561(−44)	9.363(−44)	3.427(−43)	2.831(−44)
10	1.104(−42)	1.053(−42)	2.680(−42)	1.242(−42)
20	6.965(−42)	6.285(−42)	1.547(−41)	9.562(−42)
30	1.833(−41)	1.568(−41)	4.058(−41)	2.508(−41)
40	3.555(−41)	2.885(−41)	7.995(−41)	4.685(−41)
50	5.892(−41)	4.546(−41)	1.348(−40)	7.403(−41)
60	8.839(−41)	6.495(−41)	2.338(−40)	1.057(−40)
70	1.240(−40)	8.699(−41)	2.949(−40)	1.409(−40)
80	1.657(−40)	1.111(−40)	4.036(−40)	1.790(−40)
90	2.131(−40)	1.369(−40)	5.320(−40)	2.191(−40)
100	2.657(−40)	1.640(−40)	6.631(−40)	2.606(−40)

$\epsilon$ ) are well beyond the range of applicability of all modern realistic interactions, which are typically constrained to fit  $NN$  scattering data up to pion production threshold ( $T \simeq 150 \text{ MeV}$ ). This is also the case for the AV18 of course, although it is known [40] that this interaction reproduces quite well phase shifts (at least in those channels where inelasticities are small) up to  $T \lesssim 300 \text{ MeV}$ .

As an additional caveat, we note that the present theory cannot describe the inclusive cross section in the pion-production region, for example the  $\Delta$ -excitation peak region, since no mechanisms for (real) single- or multi-pion production are included in it. However, it does reproduce quite well the observed  $d(e, e')$  inclusive cross section in the quasi-elastic peak region at intermediate values of the three-momentum transfer. This is illustrated in Fig. 1 (a-d), where the longitudinal and transverse response functions  $R_L$  and  $R_T$  obtained at Bates [41] by Rosenbluth separation of  $(e, e')$  data at momentum transfers of 300 MeV and 500 MeV are compared with theory. In these figures, we show separately the response functions calculated with an electromagnetic current including one-body only and (one+two)-body terms, as well as those obtained by replacing the fully interacting  $NN$  states of Eq. (4.6) with plane waves (curves labeled by PW). Two-body terms in  $R_L$  give negligible contributions, those in  $R_T$  lead to an increase of the transverse strength over the whole quasi-elastic region, which amounts to a few % at the top of the peak, but becomes sizable (relative to the one-body response) as the energy transfer  $\omega$  increases well beyond the quasi-elastic peak energy  $\omega_{qe} = (q^2 + m^2)^{1/2} - m$ . At these momentum transfers, the quasi-elastic and  $\Delta$  peaks in  $R_T$ , the latter at  $\omega_\Delta = (q^2 + m_\Delta^2)^{1/2} - m$  ( $m_\Delta = 1232 \text{ MeV}$ ), are well separated—note, however, the rise seen in the data at  $q = 500 \text{ MeV}$  and the highest  $\omega$ 's, presumably due to (transverse) strength creeping in from the  $\Delta$ -peak region. Interaction effects in the  $NN$  continuum states are important, particularly at low momentum transfers and/or for energy transfers close to the threshold for deuteron breakup. However, at the larger  $q$ -values plane-wave states provide response functions in the quasi-elastic region, which are fairly close to those predicted by the exact scattering states. Finally, we note that at  $q = 500 \text{ MeV}$  and quasi-elastic energies theory over-predicts the measured longitudinal response. As a consequence, the total integrated longitudinal strength—the Coulomb sum rule—obtained from these data [42] is smaller than calculated. On the other hand, there is excellent agreement between the theoretical and measured Coulomb sum rules at  $q = 300$  (and 400) MeV [42].

In Table II the columns labeled  $\nu_l$ -NC and  $\bar{\nu}_l$ -NC refer to the NC-induced reactions in Eq. (2.1), those labeled  $\nu_e$ -CC and  $\bar{\nu}_e$ -CC refer to CC-induced reactions in Eq. (2.2), and the initial neutrino energy is between 5 MeV (close to threshold) and 100 MeV. In this energy range the cross sections change rapidly, by 3–4 orders of magnitude, and interaction effects in the final scattering states are important. Two-body terms in the vector and axial pieces of the weak current increase the one-body cross section typically by a 2–3 % for both the NC- and CC-induced reactions, in agreement with the results of Ref. [12].

There are differences between the present calculations and those of Nakamura *et al.* [12]—mostly having to do with the model for the weak current—which, however, only lead to small numerical differences in the predicted cross section values, as shown below. As we have already remarked in Sec. IIIB, the authors of that work ignore the relativistic corrections proportional  $1/m^2$  in the one-body axial current (3.9), and use a different short-range parametrization for the two-body vector and axial currents than adopted here. In addition, the cutoff masses entering the nucleon form factors have slightly different values from those listed in Sec. IIIA. In order to have a more meaningful comparison with the results of that work, we have carried out a calculation of the NC- and CC-induced cross sections at three representative initial neutrino energies, in which we have removed the relativistic correction in the one-body axial current and have changed the cutoff mass values in the nucleon form factors so as to match those used in Ref. [12]. Inspection of Table V shows that the two calculations are typically within less than 1% of each other. This level of

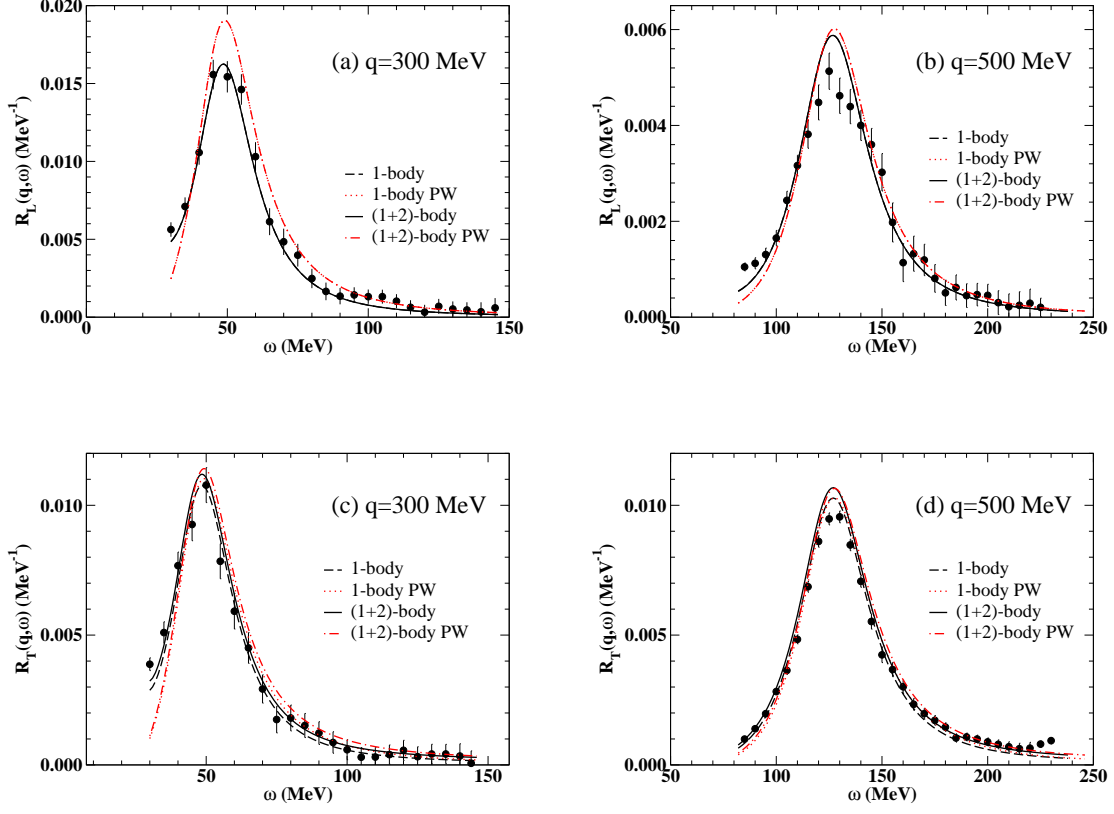


FIG. 1: (color online) The electromagnetic responses: longitudinal at  $q = 300$  MeV (a); longitudinal at  $q = 500$  MeV (b); transverse at  $q = 300$  MeV (c); transverse at  $q = 500$  MeV (d). These are obtained with the AV18 potential and the inclusion of one-body (dashed line) and (one+two)-body (solid line) terms in the nuclear electromagnetic charge operator, and are compared to data. Also shown are the results obtained with plane-wave (PW) final states.

agreement should be viewed as satisfactory, given the different ways in which the two calculations are carried out in practice. The authors of Ref. [12] rely on a multipole expansion of the cross section, whereas we compute the matrix elements entering the various response functions by direct numerical integrations, which avoid the need for introducing (cumbersome) multipole expansions of the weak transition operators. Of course, the present calculations are computationally intensive: evaluation of the NC cross sections requires about 40 mins per neutrino energy on 512 processors, and similar times for each of the two CC cross sections.

The calculated cross sections for the NC- and CC-induced reactions are listed, respectively, in Tables III and IV for incident neutrino energies between 100 MeV and 1000 MeV. The columns labeled (1,C) and (1+2,C) [(1,PW) and (1+2,PW)] show results obtained by including fully interacting [plane-wave]  $NN$  final states, and one-body only or (one+two)-body terms in the weak current. These results are also displayed in Figs. 2–5. The two-body contributions are small, less than 10% over the whole energy range. Interaction effects in the final states are found to be even smaller, which suggests that realistic estimates for these cross sections on the deuteron (and possibly nuclei with  $A > 2$ ) at high energies may be obtained by approximating the final nuclear states by plane waves, i.e. by employing the nucleon momentum distribution in the deuteron (or the spectral function in  $A > 2$  nuclei). Lastly, in Figs. 2 and 4 we also show the results obtained by including only the axial piece in the weak current. In this case, the interference response function  $R_{xy}$  vanishes, and consequently the  $\nu_l$  and  $\bar{\nu}_l$  cross sections are the same. For CC-induced reactions, due to the charge-dependence of the  $NN$  final state ( $pp$  or  $nn$ ) the neutrino-induced CC reactions has slightly larger cross section (a few %) even with only the axial piece in the weak current. We display the axial contribution in the anti-neutrino-induced CC reactions in Fig. 4. Axial contributions are larger than vector at low energy  $\lesssim (400\text{--}500)$  MeV, but become smaller than vector at higher energy.

The sensitivity of the results on the model used for the two-body axial current (Set I or Set II) and  $NN$  potential (AV18 or CD-Bonn) is investigated, respectively, in Tables VI and VII. In both cases, the model dependence is found

TABLE III: Total cross sections in  $\text{cm}^2$  for the NC-induced processes on the deuteron as function of the initial neutrino energy  $\epsilon$ , obtained with the AV18 potential and the inclusion of one-body (1) and (one+two)-body (1+2) terms in the weak current. Results corresponding to continuum final states (C) and plane wave final states (PW) are listed.

$\epsilon$ (MeV)	$\nu_l(1,C)$	$\nu_l(1+2,C)$	$\nu_l(1,PW)$	$\nu_l(1+2,PW)$	$\bar{\nu}_l(1,C)$	$\bar{\nu}_l(1+2,C)$	$\bar{\nu}_l(1,PW)$	$\bar{\nu}_l(1+2,PW)$
100	2.577(-40)	2.657(-40)	2.469(-40)	2.510(-40)	1.604(-40)	1.640(-40)	1.607(-40)	1.619(-40)
150	5.720(-40)	5.935(-40)	5.626(-40)	5.752(-40)	3.003(-40)	3.075(-40)	3.096(-40)	3.124(-40)
200	9.435(-40)	9.846(-40)	9.384(-40)	9.650(-40)	4.345(-40)	4.460(-40)	4.526(-40)	4.576(-40)
250	1.324(-39)	1.389(-39)	1.324(-39)	1.369(-39)	5.531(-40)	5.695(-40)	5.778(-40)	5.858(-40)
300	1.683(-39)	1.772(-39)	1.689(-39)	1.754(-39)	6.546(-40)	6.762(-40)	6.842(-40)	6.962(-40)
350	2.003(-39)	2.116(-39)	2.014(-39)	2.101(-39)	7.420(-40)	7.687(-40)	7.752(-40)	7.917(-40)
400	2.279(-39)	2.414(-39)	2.295(-39)	2.403(-39)	8.186(-40)	8.504(-40)	8.545(-40)	8.760(-40)
450	2.509(-39)	2.664(-39)	2.531(-39)	2.660(-39)	8.856(-40)	9.221(-40)	9.255(-40)	9.520(-40)
500	2.703(-39)	2.874(-39)	2.727(-39)	2.874(-39)	9.503(-40)	9.916(-40)	9.906(-40)	1.023(-40)
550	2.861(-39)	3.046(-39)	2.888(-39)	3.051(-39)	1.010(-39)	1.056(-39)	1.052(-39)	1.089(-39)
600	2.989(-39)	3.185(-39)	3.019(-39)	3.196(-39)	1.068(-39)	1.118(-39)	1.110(-39)	1.153(-39)
650	3.093(-39)	3.299(-39)	3.125(-39)	3.315(-39)	1.124(-39)	1.178(-39)	1.166(-39)	1.214(-39)
700	3.176(-39)	3.390(-39)	3.210(-39)	3.411(-39)	1.178(-39)	1.237(-39)	1.221(-39)	1.275(-39)
750	3.243(-39)	3.463(-39)	3.278(-39)	3.489(-39)	1.232(-39)	1.295(-39)	1.275(-39)	1.333(-39)
800	3.297(-39)	3.522(-39)	3.333(-39)	3.552(-39)	1.284(-39)	1.352(-39)	1.327(-39)	1.391(-39)
850	3.340(-39)	3.570(-39)	3.377(-39)	3.603(-39)	1.337(-39)	1.408(-39)	1.379(-39)	1.448(-39)
900	3.374(-39)	3.608(-39)	3.412(-39)	3.644(-39)	1.388(-39)	1.463(-39)	1.430(-39)	1.504(-39)
950	3.403(-39)	3.639(-39)	3.440(-39)	3.678(-39)	1.440(-39)	1.518(-39)	1.481(-39)	1.559(-39)
1000	3.425(-39)	3.663(-39)	3.461(-39)	3.704(-39)	1.490(-39)	1.572(-39)	1.530(-39)	1.613(-39)

TABLE IV: Same as in Table III, but for CC-induced processes.

$\epsilon$ (MeV)	$\bar{\nu}_e(1,C)$	$\bar{\nu}_e(1+2,C)$	$\bar{\nu}_e(1,PW)$	$\bar{\nu}_e(1+2,PW)$	$\nu_e(1,C)$	$\nu_e(1+2,C)$	$\nu_e(1,PW)$	$\nu_e(1+2,PW)$
100	2.567(-40)	2.606(-40)	2.362(-40)	2.370(-40)	6.424(-40)	6.631(-40)	5.908(-40)	6.023(-40)
150	4.688(-40)	4.751(-40)	4.487(-40)	4.491(-40)	1.516(-39)	1.574(-39)	1.440(-39)	1.477(-39)
200	6.736(-40)	6.830(-40)	6.555(-40)	6.568(-40)	2.605(-39)	2.719(-39)	2.525(-39)	2.603(-39)
250	8.677(-40)	8.822(-40)	8.520(-40)	8.567(-40)	3.775(-39)	3.958(-39)	3.699(-39)	3.833(-39)
300	1.059(-39)	1.082(-39)	1.044(-39)	1.056(-39)	4.928(-39)	5.186(-39)	4.854(-39)	5.052(-39)
350	1.254(-39)	1.286(-39)	1.239(-39)	1.261(-39)	5.981(-39)	6.315(-39)	5.923(-39)	6.189(-39)
400	1.455(-39)	1.499(-39)	1.441(-39)	1.475(-39)	6.920(-39)	7.320(-39)	6.876(-39)	7.210(-39)
450	1.663(-39)	1.722(-39)	1.650(-39)	1.698(-39)	7.778(-39)	8.248(-39)	7.704(-39)	8.102(-39)
500	1.879(-39)	1.952(-39)	1.865(-39)	1.930(-39)	8.524(-39)	9.053(-39)	8.410(-39)	8.868(-39)
550	2.100(-39)	2.189(-39)	2.087(-39)	2.169(-39)	9.064(-39)	9.636(-39)	9.005(-39)	9.519(-39)
600	2.323(-39)	2.428(-39)	2.309(-39)	2.410(-39)	9.556(-39)	1.017(-38)	9.504(-39)	1.007(-38)
650	2.548(-39)	2.671(-39)	2.537(-39)	2.656(-39)	9.966(-39)	1.062(-38)	9.920(-39)	1.053(-38)
700	2.777(-39)	2.916(-39)	2.766(-39)	2.905(-39)	1.031(-38)	1.098(-38)	1.027(-38)	1.091(-38)
750	3.005(-39)	3.161(-39)	2.995(-39)	3.152(-39)	1.059(-38)	1.129(-38)	1.055(-38)	1.124(-38)
800	3.232(-39)	3.403(-39)	3.223(-39)	3.399(-39)	1.082(-38)	1.154(-38)	1.079(-38)	1.150(-38)
850	3.456(-39)	3.645(-39)	3.448(-39)	3.643(-39)	1.101(-38)	1.176(-38)	1.099(-38)	1.173(-38)
900	3.678(-39)	3.882(-39)	3.671(-39)	3.885(-39)	1.118(-38)	1.193(-38)	1.116(-38)	1.192(-38)
950	3.896(-39)	4.116(-39)	3.890(-39)	4.122(-39)	1.131(-38)	1.208(-38)	1.129(-38)	1.208(-38)
1000	4.109(-39)	4.343(-39)	4.105(-39)	4.356(-39)	1.142(-38)	1.221(-38)	1.141(-38)	1.222(-38)

to be negligible. The two-body vector currents are taken from the AV18, and therefore their short-range behavior is not consistent with the CD-Bonn interaction. This inconsistency, though, is of little numerical import. Furthermore, since interaction effects in the two-nucleon continuum appear to be negligible for neutrino energies  $\gtrsim 100$  MeV, the agreement between the calculated cross sections with the AV18 and CD-Bonn merely reflects the fact that the momentum distributions predicted by these two potential models are very close to each other for relative momenta  $\lesssim 400$  MeV.

In Figs. 6–14 we show the differential cross sections for the NC- and CC-induced reactions as function of the final lepton energy  $\epsilon'$  and scattering angle  $\theta$  at three incident neutrino energies,  $\epsilon = 100, 500, 900$  MeV. The quasi-elastic peak is located at a final energy  $\epsilon'_{\text{qe}}$  given by

$$\epsilon'_{\text{qe}} = \frac{\epsilon}{1 + (2\epsilon/m) \sin^2 \theta/2}, \quad (5.1)$$

where we have neglected the lepton mass in the case of the CC processes. Therefore as  $\theta$  changes from the backward

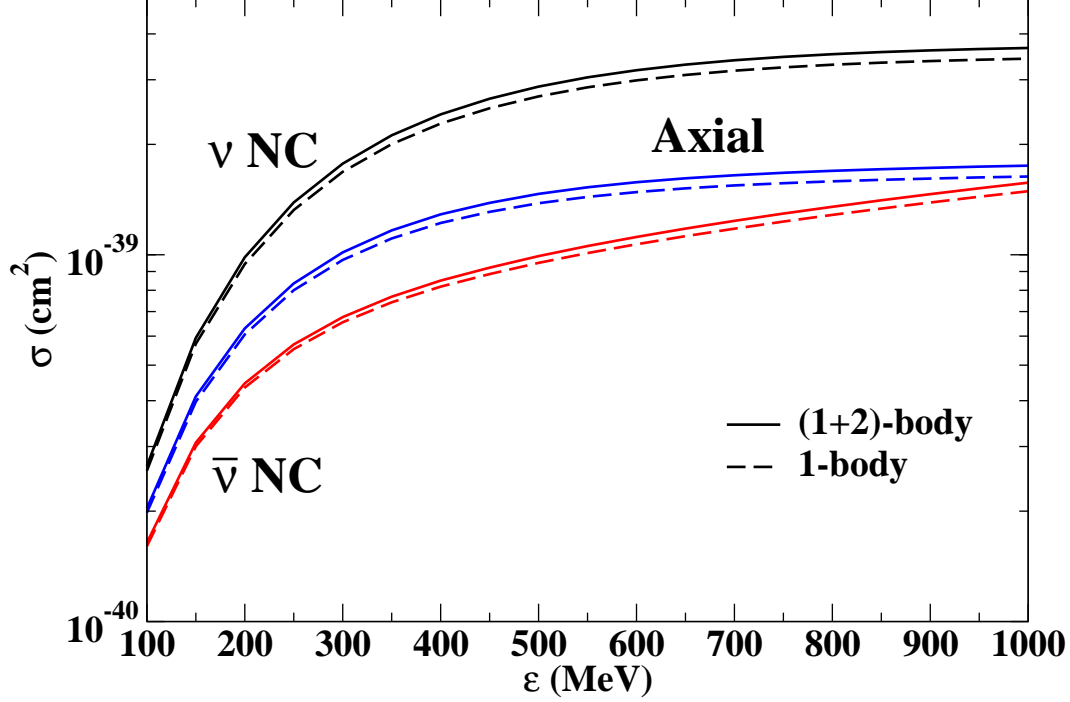


FIG. 2: (color online) Total cross sections for NC-induced processes on the deuteron, obtained with the AV18 potential and the inclusion of one-body (dashed line) and (one+two)-body (solid line) terms in the weak current. Also shown are the total cross sections obtained by retaining only the axial piece of the weak current. See text for explanation.

TABLE V: (color on line) Total cross sections in  $\text{cm}^2$  for the NC- and CC-induced processes on the deuteron obtained in Ref. [12] and in the present work at selected initial neutrino energies. Note that the values under the heading “this work” are slightly different than those reported in Table II for the reasons explained in the text.

$\epsilon$ (MeV)	5		50		100	
	Ref. [12]	this work	Ref. [12]	this work	Ref. [12]	this work
$\nu_l\text{-NC}$	9.570(−44)	9.601(−44)	5.944(−41)	5.942(−41)	2.711(−40)	2.703(−40)
$\bar{\nu}_l\text{-NC}$	9.364(−44)	9.403(−44)	4.535(−41)	4.589(−41)	1.647(−40)	1.674(−40)
$\nu_e\text{-CC}$	3.463(−43)	3.440(−43)	1.376(−40)	1.367(−40)	6.836(−40)	6.735(−40)
$\bar{\nu}_e\text{-CC}$	2.836(−44)	2.842(−44)	7.372(−41)	7.475(−41)	2.618(−40)	2.659(−40)

to the forward hemisphere, the quasi-elastic peak moves to the right, i.e. towards higher and higher energies. Indeed, at forward angles it merges with the threshold peak due to the quasi-bound  $^1\text{S}_0$  state. This latter peak is very pronounced at low  $\epsilon$ , but becomes more and more suppressed by the form factor  $\sim \langle ^1\text{S}_0 | j_0(qr/2) | d \rangle$  as  $\epsilon$  increases.

Finally, it is interesting to compare the results above with those obtained in a naive model, in which the deuteron is taken to consist of a free proton and neutron initially at rest. The lab-frame cross sections of the NC-induced processes on the nucleon, and of the CC-induced processes  $n(\nu_e, e^-)p$  and  $p(\bar{\nu}_e, e^+)n$  in the limit in which the final electron/positron mass and proton-neutron mass difference are neglected, read [43]:

$$\left( \frac{d\sigma}{d\epsilon' d\Omega} \right)_{\nu/\bar{\nu}}^{\text{NC/CC}} = \frac{G^2 m^2}{8\pi^2} \left( \frac{\epsilon'}{\epsilon} \right)^2 \delta(\epsilon' - \epsilon'_{\text{qe}}) \left[ A^{\text{NC/CC}} \mp \frac{s-u}{m^2} B^{\text{NC/CC}} + \frac{(s-u)^2}{m^4} C^{\text{NC/CC}} \right], \quad (5.2)$$

where  $G=G_F$  or  $G_F \cos \theta_C$  for NC or CC, the  $- (+)$  sign in the second term is relative to the  $\nu$  ( $\bar{\nu}$ ) initiated reactions,  $\epsilon'_{\text{qe}}$  has been defined in Eq. (5.1), and  $s-u = 4m\epsilon - Q^2$  with  $Q^2 = 4\epsilon\epsilon' \sin^2 \theta/2$ . The structure functions  $A(Q^2)$ ,



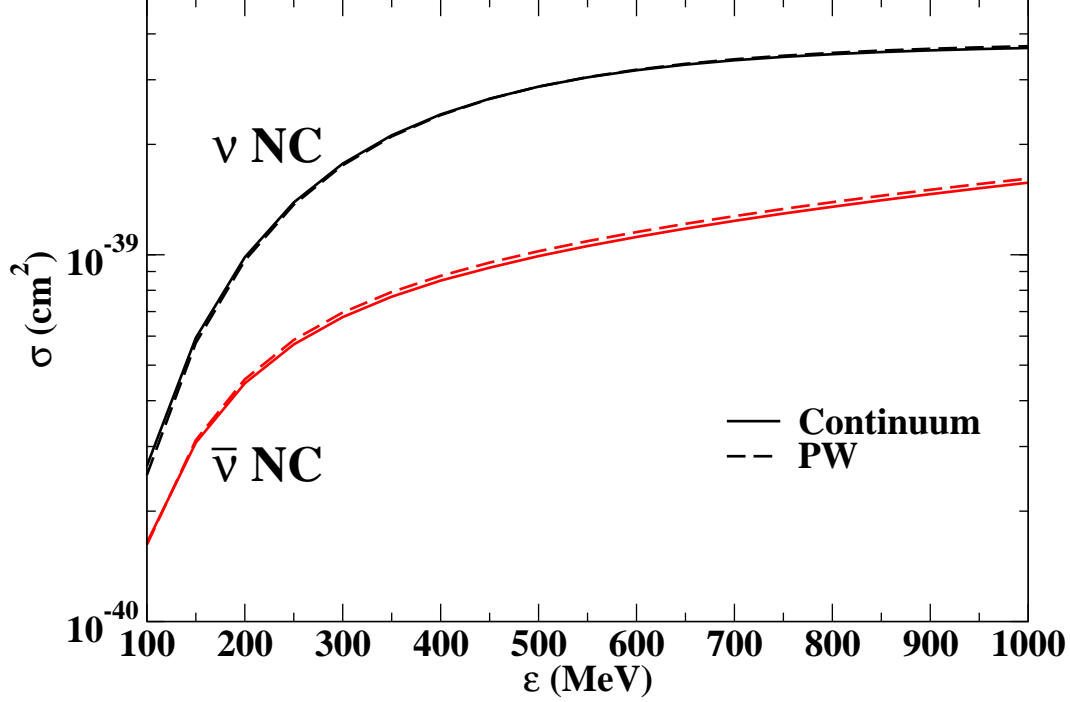


FIG. 3: (color online) Total cross sections for NC-induced processes on the deuteron, obtained with the AV18 potential and the inclusion of (one+two)-body terms in the weak current. Also shown are the total cross sections obtained with plane-wave (PW) final states.

TABLE VI: Total cross sections in  $\text{cm}^2$  for the NC- and CC-induced processes on the deuteron at selected initial neutrino energies, obtained with the AV18 potential and the inclusion of one-body and set I or set II two-body terms in the weak current.

$\epsilon$ (MeV)	$\nu_l$ -NC		$\bar{\nu}_l$ -NC		$\nu_e$ -CC		$\bar{\nu}_e$ -CC	
	set I	set II	set I	set II	set I	set II	set I	set II
5	9.561(-44)	9.541(-44)	9.363(-44)	9.344(-44)	3.427(-43)	3.421(-43)	2.831(-44)	2.826(-44)
50	5.892(-41)	5.873(-41)	4.546(-41)	4.530(-41)	1.348(-40)	1.353(-40)	7.403(-41)	7.380(-41)
100	2.657(-40)	2.652(-40)	1.640(-40)	1.636(-40)	6.631(-40)	6.621(-40)	2.606(-40)	2.600(-40)

$B(Q^2)$ , and  $C(Q^2)$  for both NC and CC are given in terms of nucleon form factors in Appendix B.

In the naive model, the  $\nu$ - and  $\bar{\nu}$ -deuteron NC cross sections are simply given by the sum of the corresponding proton and neutron (NC) cross sections, while the  $\nu$ -deuteron ( $\bar{\nu}$ -deuteron) CC cross section is identified with the  $n(\nu_e, e^-)p$  [ $p(\bar{\nu}_e, e^+)n$ ] cross section. The “model” differential cross sections as function of the final lepton scattering angle (after integrating out the energy-conserving  $\delta$ -function) are illustrated in Fig. 15 at three incident energies ( $\epsilon = 100, 500, 900$  MeV). The  $\nu$  and  $\bar{\nu}$  cross sections are about the same at forward angles, for which  $Q^2$  is small; at backward angles, as  $\epsilon$  and  $Q^2$  increase, they both decrease due to the fall off in the form factors. However, this fall off is much more pronounced (orders of magnitude) for the  $\bar{\nu}$  than for the  $\nu$  cross sections. (At low energy 100 MeV, the form factors do not change much with angle and the variation with angle in the differential cross section is mild, still it decreases more in the  $\bar{\nu}$  than in  $\nu$  channel.) These features are reflected in the deuteron cross sections displayed in Figs. 6–14 (incidentally, in each panel of these figures the “model” cross sections would be represented by a  $\delta$ -function located at  $\epsilon'_{qe}$ , corresponding to the energy of the quasi-elastic peak).

In order to illustrate nuclear correlation effects in the initial deuteron state, we compare the “model”  $\nu$  and  $\bar{\nu}$  NC

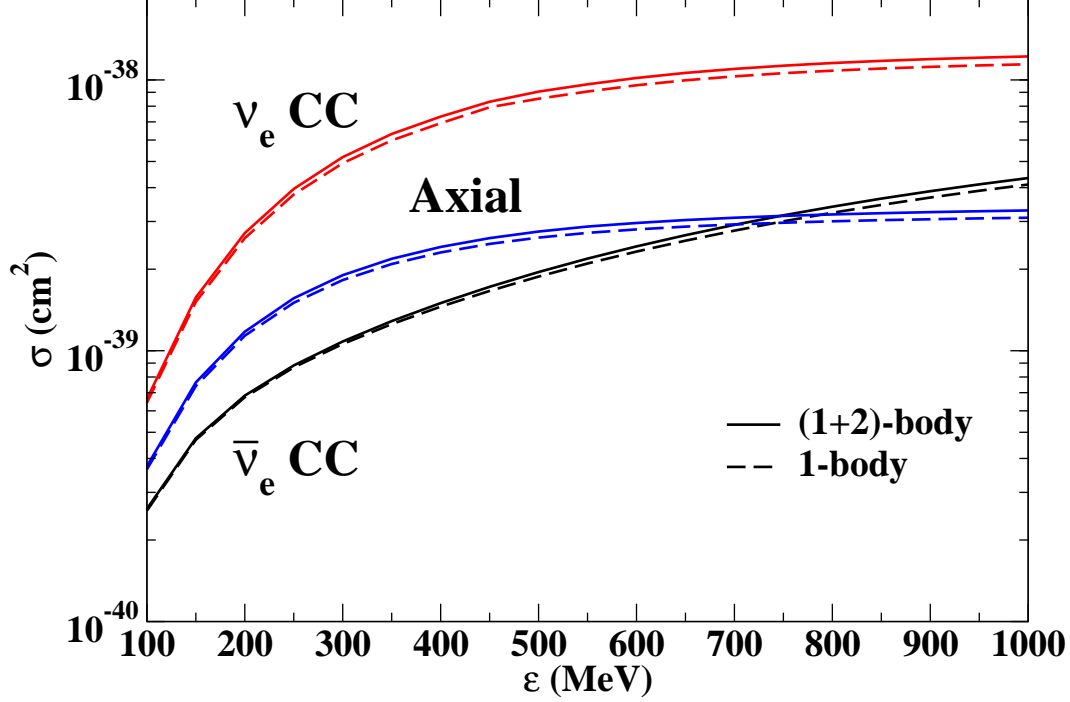


FIG. 4: (color online) Same as in Fig. 2, but for CC-induced processes on the deuteron.

TABLE VII: Total cross sections in  $\text{cm}^2$  for the NC-induced processes on the deuteron at selected initial neutrino energies, obtained with the AV18 or CDB potentials and the inclusion of one-body terms (1) only and both one- and two-body terms (1+2) in the weak current.

	$\nu_l\text{-NC}$				$\bar{\nu}_l\text{-NC}$			
$\epsilon$ (MeV)	AV18(1)	CDB(1)	AV18(1+2)	CDB(1+2)	AV18(1)	CDB(1)	AV18(1+2)	CDB(1+2)
50	5.747(−41)	5.791(−40)	5.892(−41)	5.847(−40)	4.449(−41)	4.484(−40)	4.546(−41)	4.519(−40)
100	2.577(−40)	2.597(−40)	2.657(−40)	2.638(−40)	1.604(−40)	1.617(−40)	1.640(−40)	1.633(−40)
500	2.703(−39)	2.715(−39)	2.874(−39)	2.858(−39)	9.503(−40)	9.553(−40)	9.916(−40)	9.895(−40)
1000	3.425(−39)	3.442(−39)	3.663(−39)	3.659(−39)	1.490(−39)	1.496(−39)	1.572(−39)	1.572(−39)

cross sections with the plane-wave one-body results, shown in Fig. 16, for which we use the physical deuteron state, plane waves for the two-nucleon continuum states, and one-body currents. In both  $\nu$  and  $\bar{\nu}$  NC reactions, inclusion of nuclear correlations in the initial state reduces the cross sections from the naive model. In fact, a similar reduction in cross section (due to nuclear correlations) at about nuclear density for uniform nuclear matter has been noticed, for example in Refs. [44, 45]. However, these correlations increase the ratio of  $\nu$  to  $\bar{\nu}$  NC cross sections, as shown in the inset of Fig. 16. Similar effects are also found in the  $\nu$  and  $\bar{\nu}$  CC reactions at low neutrino energy, as shown in Fig. 17. At higher energies, nuclear correlations hardly affect these cross sections, and the naive and realistic models are in better agreement with each other. The ratio of  $\nu$  to  $\bar{\nu}$  CC cross sections is also increased due to nuclear correlations (see inset of Fig. 17). This fact may have interesting implications for long baseline neutrino experiments aimed at extracting CP violating signals from the detection of differences in the neutrino and antineutrino channels.

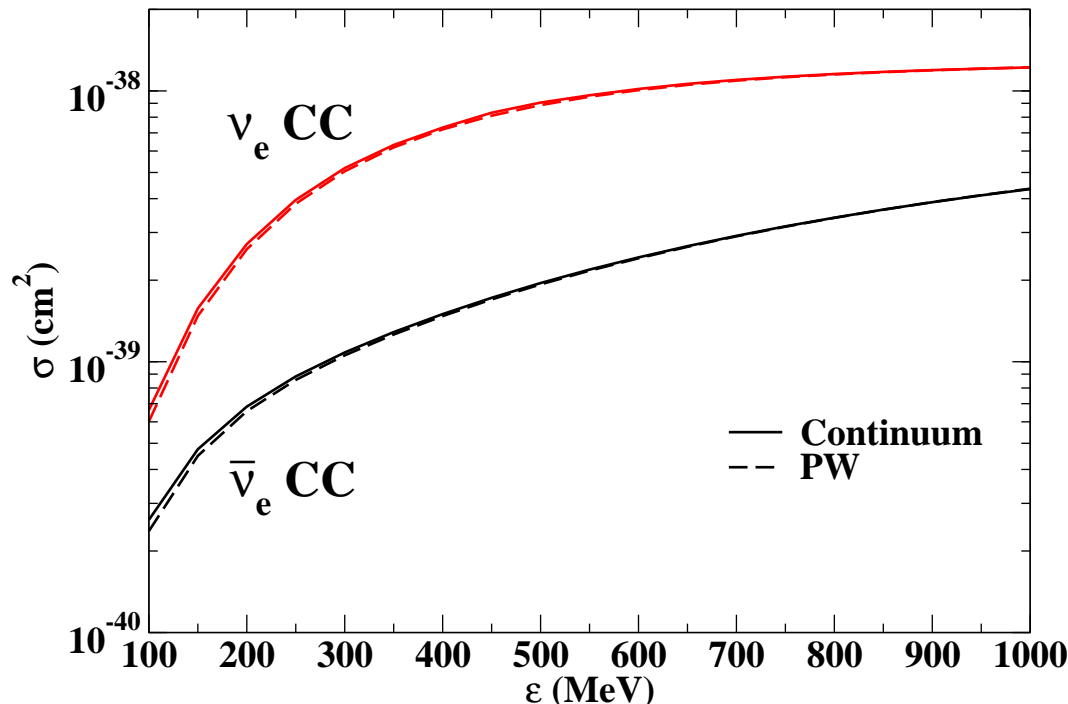


FIG. 5: (color online) Same as in Fig. 3, but for CC-induced processes on the deuteron.

## VI. CONCLUSIONS AND OUTLOOK

In this work, we have studied inclusive neutrino scattering on the deuteron up to neutrino energies of 1 GeV, by using a realistic description of two-nucleon interactions and weak currents. Two-body terms in the latter increase the calculated cross sections with one-body currents by less than 10% over the whole energy region for both the NC- and CC-induced processes. Interaction effects in the two-nucleon continuum final state are found to be negligible for neutrino energies  $\gtrsim 500$  MeV. This suggests that fairly realistic estimates for these cross sections in light nuclei (and at relatively high neutrino energies) may be obtained in calculations based on the plane-wave impulse approximation. Even calculations in this limit, however, cannot be presently carried out, as they require knowledge of nuclear spectral functions over a wide range of missing momenta and energies—these are not yet available in light nuclei. Nuclear correlation effects in the initial deuteron state are found to be important. They reduce the  $\nu$  and, to a larger extent,  $\bar{\nu}$  cross sections over the whole range of energies studied in this work, and therefore significantly increase the  $\nu$  to  $\bar{\nu}$  cross-section ratio for both NC and CC reactions. In the present work the pion-production channels are not included. Experimentally they produce distinctive final states and give important contributions to total neutrino cross sections above pion-production threshold. It would be interesting to include these channels in future.

It should be possible to use quantum Monte Carlo (QMC) methods [15] to study neutrino response functions, and associated sum rules, in light nuclei within the same (realistic) dynamical framework adopted here. Indeed, “exact” calculations of this type [46] led to a quantitatively accurate description of the quasi-elastic electromagnetic response functions measured in  $A = 3$  and 4 nuclei. In particular, they showed that the charge-exchange character of the nucleon-nucleon interaction leads to shifts of longitudinal and transverse strength at higher excitation energies, thus providing a quenching of the response in the quasi-elastic peak region. This mechanism, however, is more than offset in the transverse channel by two-body currents, in particular those associated with pion exchange, and hence the response is enhanced over the entire quasi-elastic spectrum. It will be interesting to see the extent to which these considerations will remain valid in the weak sector probed in neutrino scattering, and possibly provide an explanation for the observed anomaly in the  $^{12}\text{C}$  data.

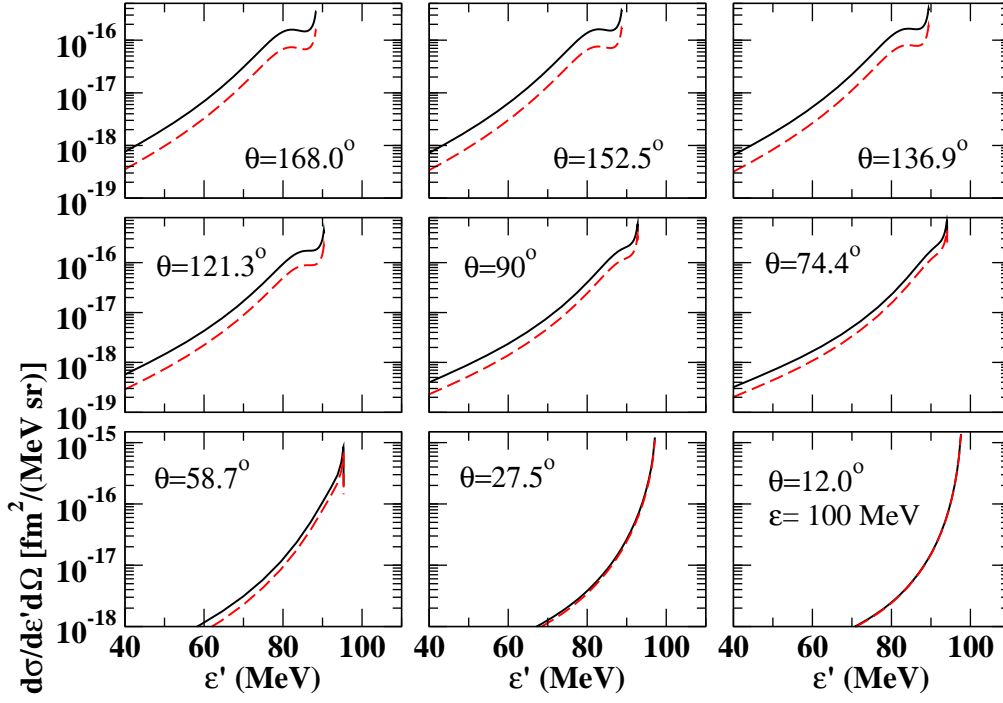


FIG. 6: (color online) Differential cross section for NC-induced processes on the deuteron, obtained with the AV18 potential and the inclusion of one- and two-body terms in the nuclear weak current, as function of final lepton energy. The incident neutrino energy is 100 MeV. The final lepton angle is indicated in each panel. The (black) solid curve is for neutrino induced processes. The (red) dashed curve is for anti-neutrino induced processes.

### Acknowledgments

It is a pleasure to thank S. Nakamura for discussions and clarifications in reference to his work on the same topic. The work of R.S. is supported by the U.S. Department of Energy, Office of Nuclear Science, under contract DE-AC05-06OR23177. This work was supported in part by a grant from the DOE under contract DE-AC52-06NA25396. The calculations were made possible by grants of computing time from the National Energy Research Supercomputer Center.

### Appendix A

The cross section for CC processes at small incident neutrino energies in which the lepton mass cannot be neglected reads

$$\left( \frac{d\sigma}{d\epsilon'd\Omega} \right)_{\nu/\bar{\nu}} = \frac{G^2}{8\pi^2} \frac{k'}{\epsilon} F(Z, k') \left[ v_{00} R_{00} + v_{zz} R_{zz} - v_{0z} R_{0z} + v_{xx+yy} R_{xx+yy} \mp v_{xy} R_{xy} \right], \quad (\text{A1})$$

where the kinematical factors are given by

$$v_{00} = 2\epsilon\epsilon' \left( 1 + \frac{k'}{\epsilon'} \cos\theta \right), \quad (\text{A2})$$

$$v_{zz} = \frac{\omega^2}{q^2} \left[ m_l^2 + 2\epsilon\epsilon' \left( 1 + \frac{k'}{\epsilon'} \cos\theta \right) \right] + \frac{m_l^2}{q^2} [m_l^2 + 2\omega(\epsilon + \epsilon') + q^2], \quad (\text{A3})$$

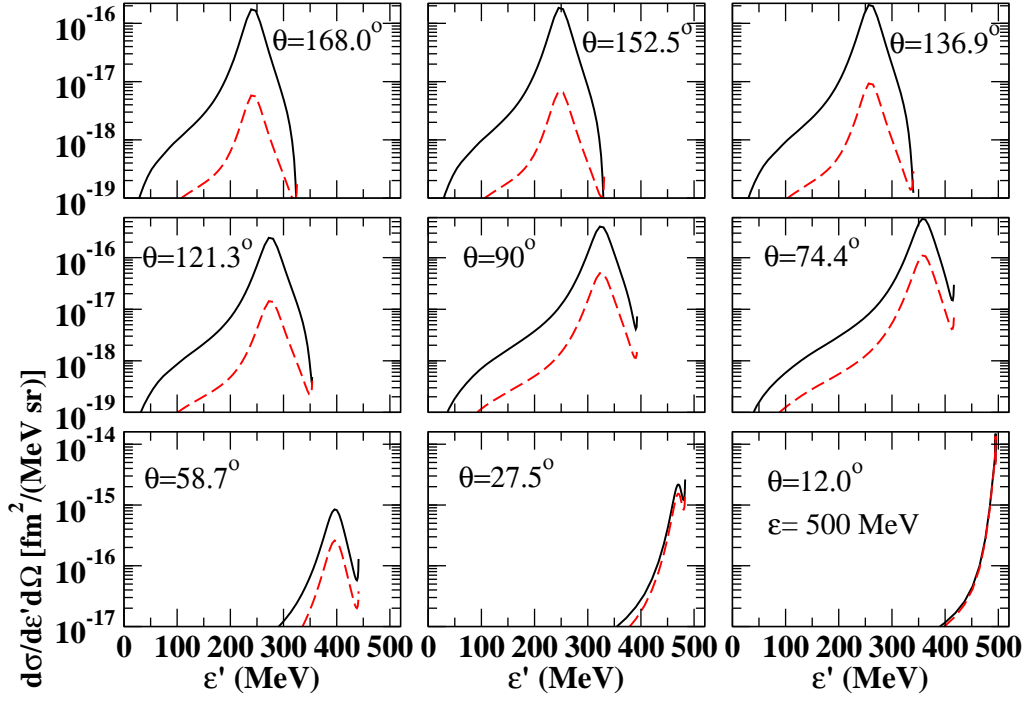


FIG. 7: (color online) Same as Fig. 6, but the incident neutrino energy is 500 MeV.

$$v_{0z} = \frac{\omega}{q} \left[ m_l^2 + 2\epsilon\epsilon' \left( 1 + \frac{k'}{\epsilon'} \cos \theta \right) \right] + m_l^2 \frac{\epsilon + \epsilon'}{q}, \quad (\text{A4})$$

$$v_{xx+yy} = Q^2 + \frac{Q^2}{2q^2} \left[ m_l^2 + 2\epsilon\epsilon' \left( 1 + \frac{k'}{\epsilon'} \cos \theta \right) \right] - \frac{m_l^2}{q^2} \left[ \frac{m_l^2}{2} + \omega(\epsilon' + \epsilon) \right], \quad (\text{A5})$$

$$v_{xy} = Q^2 \frac{\epsilon + \epsilon'}{q} - m_l^2 \frac{\omega}{q}, \quad (\text{A6})$$

$m_l$  is the final lepton mass, and the response functions are defined as in Eqs. (2.5)–(2.9). Note that

$$\epsilon + \epsilon' = \sqrt{2m_l^2 + (\mathbf{k} + \mathbf{k}')^2 + Q^2}, \quad (\text{A7})$$

and the cross section above is easily shown to reduce to Eq. (2.3) in the limit  $m_l = 0$  and  $Q^2 = 4\epsilon\epsilon' \sin^2 \theta/2$ .

## Appendix B

In this appendix, the structure functions entering the NC- and CC-induced processes on the nucleon are expressed in terms of (nucleon) form factors. In the NC case, they read:

$$A^{\text{NC}} = 4\eta \left[ (1+\eta) \left( \bar{F}_A^N \right)^2 - (1-\eta) \left( \bar{F}_1^N \right)^2 + \eta(1-\eta) \left( \bar{F}_2^N \right)^2 + 4\eta \bar{F}_1^N \bar{F}_2^N \right], \quad (\text{B1})$$

$$B^{\text{NC}} = 4\eta \bar{F}_A^N \left( \bar{F}_1^N + \bar{F}_2^N \right), \quad (\text{B2})$$

$$C^{\text{NC}} = \frac{1}{4} \left[ \left( \bar{F}_A^N \right)^2 + \left( \bar{F}_1^N \right)^2 + \eta \left( \bar{F}_2^N \right)^2 \right], \quad (\text{B3})$$

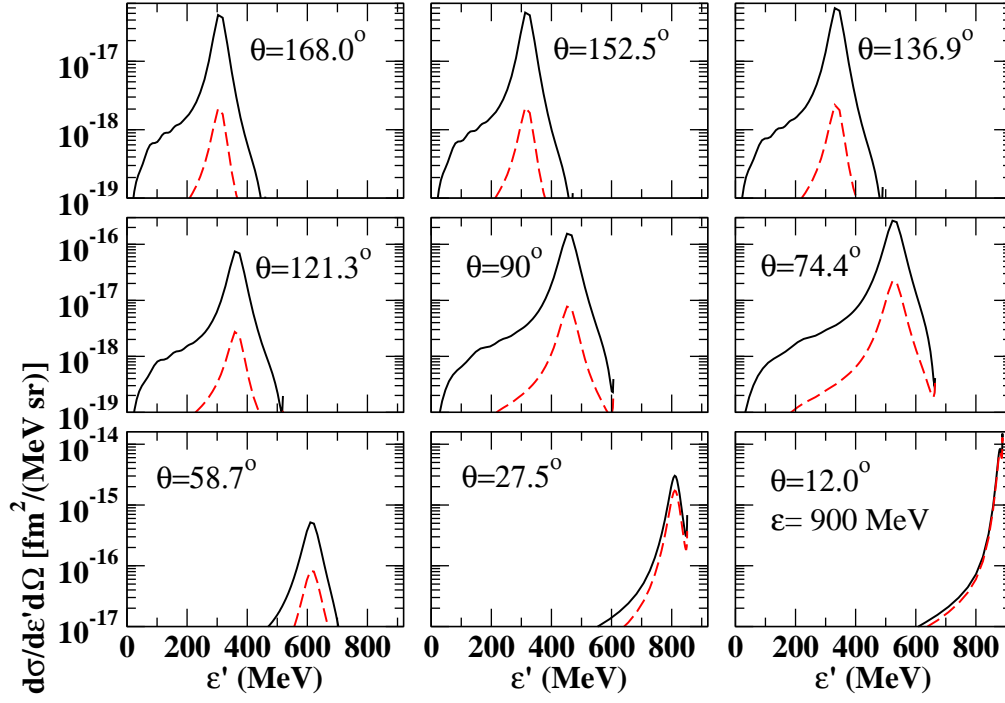


FIG. 8: (color online) Same as Fig. 6, but the incident neutrino energy is 900 MeV.

and  $\eta = Q^2/(4m^2)$ . The nucleon form factors  $\bar{F}_i^N$  and  $\bar{F}_A^N$  for  $N = p$  or  $n$  are defined as

$$2\bar{F}_i^{p/n} = (1 - 4\sin^2\theta_W)F_i^{p/n} - F_i^{n/p}, \quad (\text{B4})$$

$$2\bar{F}_A^{p/n} = \mp G_A, \quad (\text{B5})$$

where the proton and neutron electromagnetic form factors are, respectively,  $F_i^p = (F_i^S + F_i^V)/2$  and  $F_i^n = (F_i^S - F_i^V)/2$  with  $F_i^{S/V}$  defined in Eqs. (3.43)–(3.44), and the axial form factor  $G_A$  (with  $-$  for  $p$  and  $+$  for  $n$ ) as defined in Eq. (3.12). In the limit in which the final lepton mass and proton-neutron mass difference are both neglected, the relations for the  $A$ ,  $B$  and  $C$  structure functions remain valid for the CC case, provided

$$\bar{F}_i^N \longrightarrow F_i^V, \quad \bar{F}_A^N \longrightarrow G_A. \quad (\text{B6})$$

- 
- [1] A.A. Aguilar-Arevalo *et al.*, Phys. Rev. Lett. **100**, 032301 (2008).
  - [2] A.V. Butkevich, Phys. Rev. C **82**, 055501 (2010).
  - [3] O. Benhar, P. Coletti, and D. Meloni, Phys. Rev. Lett. **105**, 132301 (2010).
  - [4] C. Juszczak, J.T. Sobczyk, and J. Zmuda, Phys. Rev. C **82**, 045502 (2010).
  - [5] E. Amaldi, S. Fubini, and G. Furlan, *Electroproduction at Low Energy and Hadron Form Factors* (Springer Tracts in Modern Physics No. 83, 1979), p.1.
  - [6] N.J. Baker *et al.*, Phys. Rev. D **23**, 2499 (1981); K.L. Miller *et al.*, Phys. Rev. D **26**, 537 (1982).
  - [7] T. Kitagaki *et al.*, Phys. Rev. D **28**, 436 (1983).
  - [8] L.A. Ahrens *et al.*, Phys. Rev. D **35**, 785 (1987).
  - [9] G. Garvey, private communication.

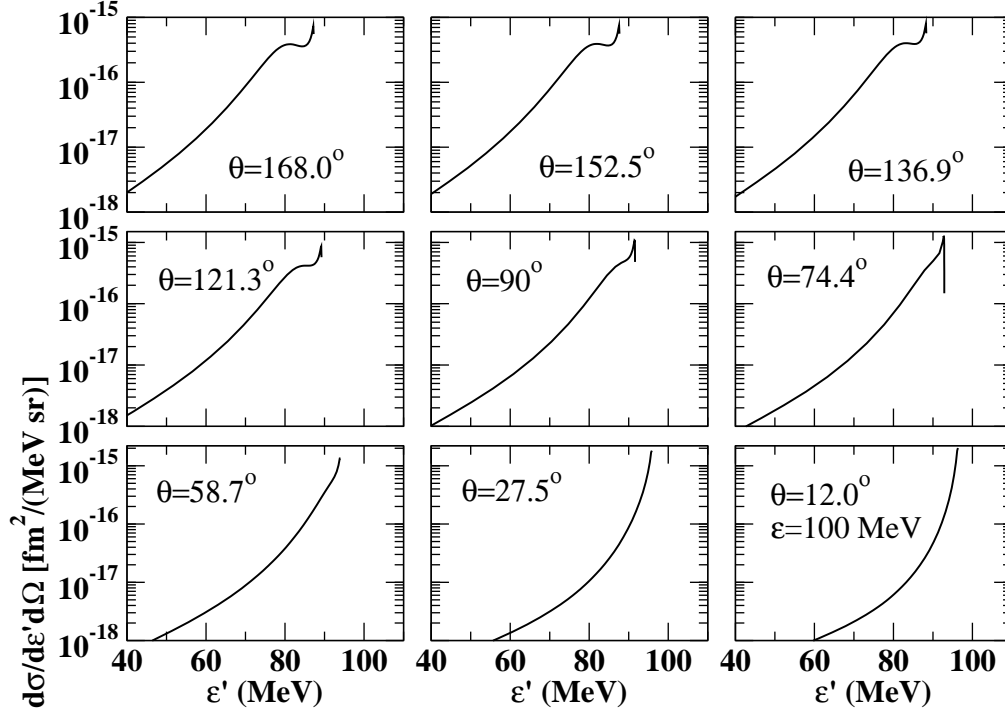


FIG. 9: Differential cross section for electron anti-neutrino induced CC processes on the deuteron, obtained with the AV18 potential and the inclusion of one- and two-body terms in the nuclear weak current, as function of final lepton energy. The incident anti-neutrino energy is 100 MeV. The final lepton angle is indicated in each panel.

- [10] K. Kubodera and S. Nozawa, *Int. J. Mod. Phys. E* **3**, 101 (1994).
- [11] S. Nakamura, T. Sato, V. Gudkov, and K. Kubodera, *Phys. Rev. C* **63**, 034617 (2001).
- [12] S. Nakamura *et al.*, *Nucl. Phys.* **A707**, 561 (2002); <http://www.physics.sc.edu/gudkov/NU-D-NSGK/>.
- [13] Q.R. Ahmad *et al.* (SNO Collaboration), *Phys. Rev. Lett.* **89**, 011301 (2002); S.N. Ahmed *et al.* (SNO Collaboration), *Phys. Rev. Lett.* **92**, 181301 (2004).
- [14] J.N. Bahcall and M.H. Pinsonneault, *Phys. Rev. Lett.* **92**, 121301 (2004).
- [15] J. Carlson and R. Schiavilla, *Phys. Rev. Lett.* **68**, 3682 (1992); *Phys. Rev. C* **49**, R2880 (1994).
- [16] I.S. Towner and J.C. Hardy, *Physics Beyond the Standard Model* (World Scientific, Singapore, 1999), P. Herczeg, C.M. Hoffman, and H.V. Klapdor-Kleingrothaus, Eds., p. 338.
- [17] K. Nakamura *et al.* (Particle Data Group), *J. Phys. G* **37**, 075021 (2010).
- [18] I.S. Towner, *Phys. Rev. C* **58**, 1288 (1998).
- [19] A. Kurylov, M.J. Ramsey-Musolf, and P. Vogel, *Phys. Rev. C* **65**, 055501 (2002); *Phys. Rev. C* **67**, 035502 (2003).
- [20] D.T. Spayde *et al.* (SAMPLE Collaboration), *Phys. Rev. Lett.* **84**, 1106 (2000); *Phys. Lett.* **B583**, 79 (2004); E.J. Beise, M.L. Pitt, and D.T. Spayde, *Prog. Part. Nucl. Phys.* **54**, 289 (2005).
- [21] Z. Ahmed *et al.* (HAPPEX Collaboration), *Phys. Rev. Lett.* **108**, 102001 (2012); K.A. Aniol *et al.* (HAPPEX Collaboration), *Phys. Rev. C* **69**, 065501 (2004); A. Acha *et al.* (HAPPEX Collaboration), *Phys. Rev. Lett.* **98**, 032301 (2007).
- [22] C.E. Hyde-Wright and K. de Jager, *Ann. Rev. Nucl. Part. Sci.* **54**, 217 (2004).
- [23] T. Gorringer and H.W. Fearing, *Rev. Mod. Phys.* **76**, 31 (2004); P. Kammel and K. Kubodera, *Ann. Rev. Nucl. Part. Sci.* **60**, 327 (2010).
- [24] A. Czarnecki, W.J. Marciano, and A. Sirlin, *Phys. Rev. Lett.* **99**, 032003 (2007).
- [25] L. E. Marcucci, A. Kievsky, S. Rosati, R. Schiavilla, and M. Viviani, *Phys. Rev. Lett.* **108**, 052502 (2012); L. E. Marcucci, M. Piarulli, M. Viviani, L. Girlanda, A. Kievsky, S. Rosati, and R. Schiavilla *Phys. Rev. C* **83**, 014002 (2011).
- [26] V.A. Andreev *et al.*, *Phys. Rev. Lett.* **99**, 032002 (2007).
- [27] P. Ackerbauer *et al.*, *Phys. Lett. B* **417**, 224 (1998).
- [28] V. Bernard, N. Kaiser, and Ulf-G. Meissner, *Phys. Rev. D* **50**, 6899 (1994); N. Kaiser, *Phys. Rev. C* **67**, 027002 (2003).

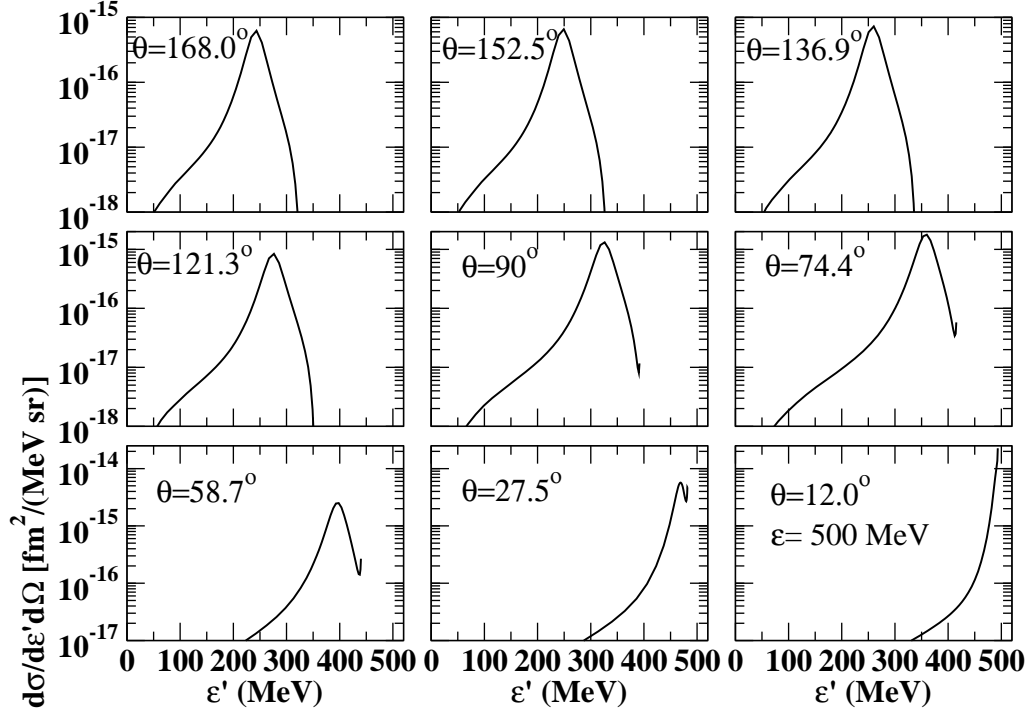


FIG. 10: Same as Fig. 9, but the incident neutrino energy is 500 MeV.

- [29] J. Carlson and R. Schiavilla, *Rev. Mod. Phys.* **70**, 743 (1998).
- [30] L.E. Marcucci, R. Schiavilla, M. Viviani, A. Kievsky, S. Rosati, and J. F. Beacom, *Phys. Rev. C* **63**, 015801 (2000).
- [31] L. E. Marcucci, M. Viviani, R. Schiavilla, A. Kievsky, and S. Rosati, *Phys. Rev. C* **72**, 014001 (2005).
- [32] C.E. Carlson, *Phys. Rev. D* **34**, 2704 (1986).
- [33] J. Carlson, V.R. Pandharipande, and R. Schiavilla, *Modern Topics in Electron Scattering* (World Scientific, Singapore, 1991), B. Frois and I. Sick, Eds., p. 177.
- [34] R. Machleidt, *Phys. Rev. C* **63**, 024001 (2001).
- [35] K. Kubodera, J. Delorme, and M. Rho, *Phys. Rev. Lett.* **40**, 755 (1978).
- [36] R. Schiavilla, J. Carlson, and M. Paris, *Phys. Rev. C* **70**, 044007 (2004).
- [37] W. Glöckle, *The Quantum Mechanical Few-Body Problem* (Springer-Verlag, Berlin, 1983).
- [38] C.M. Vincent and S.C. Phatak, *Phys. Rev. C* **10**, 391 (1974).
- [39] J. Carlson, R. Schiavilla, V.R. Brown, and B.F. Gibson, *Phys. Rev. C* **65**, 035502 (2002).
- [40] R.B. Wiringa, [www.phy.anl.gov/theory/research/av18/](http://www.phy.anl.gov/theory/research/av18/).
- [41] S.A. Dytman *et al.*, *Phys. Rev. C* **38**, 800 (1988).
- [42] R. Schiavilla, V.R. Pandharipande, and A. Fabrocini, *Phys. Rev.* **40**, 1484 (1989).
- [43] A.W. Thomas and W. Weise, *The Structure of the Nucleon* (WILEY-VCH Verlag, Berlin, 2001).
- [44] C.J. Horowitz and K. Wehrberger, *Nucl. Phys. A* **531**, 665 (1991).
- [45] S. Reddy, M. Prakash, J.M. Lattimer, and J. A. Pons, *Phys. Rev. C* **59**, 2888 (1999).
- [46] J. Carlson, J. Jourdan, R. Schiavilla, and I. Sick, *Phys. Rev. C* **65**, 024002 (2002).



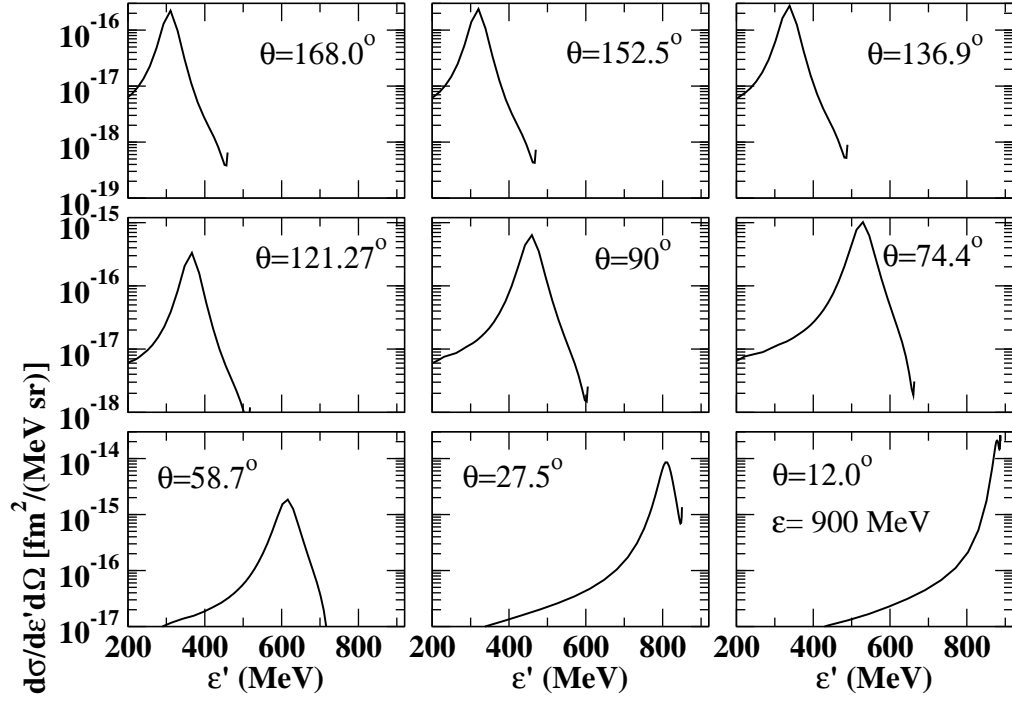


FIG. 11: Same as Fig. 9, but the incident neutrino energy is 900 MeV.

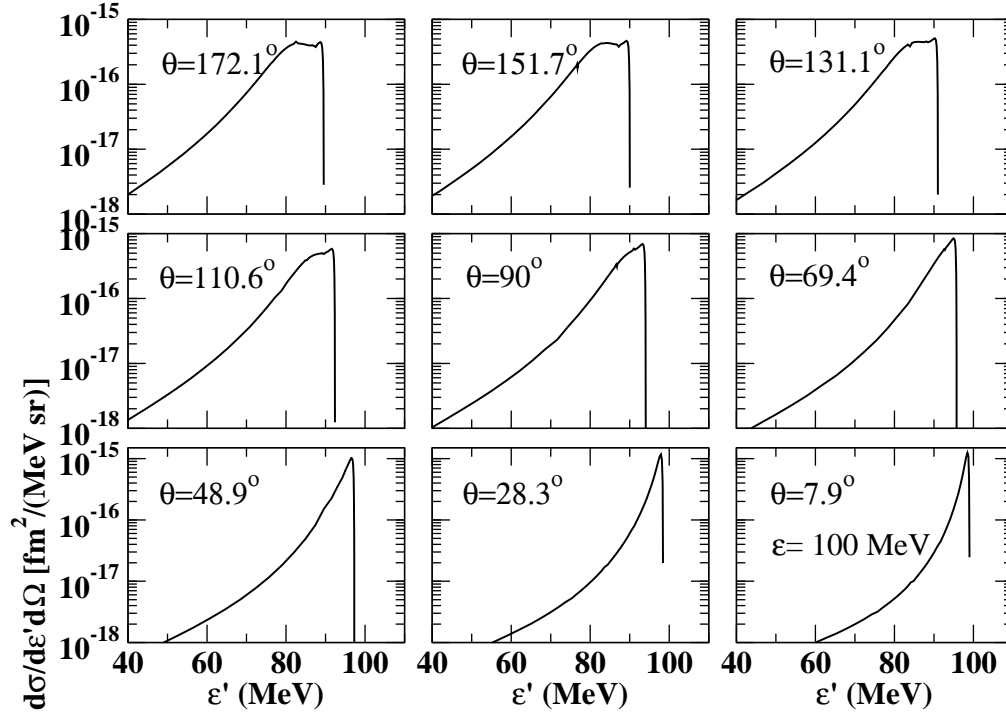


FIG. 12: Differential cross section for electron neutrino induced CC processes on the deuteron, obtained with the AV18 potential and the inclusion of one- and two-body terms in the nuclear weak current, as function of final lepton energy. The incident neutrino energy is 100 MeV. The final lepton angle is indicated in each panel.

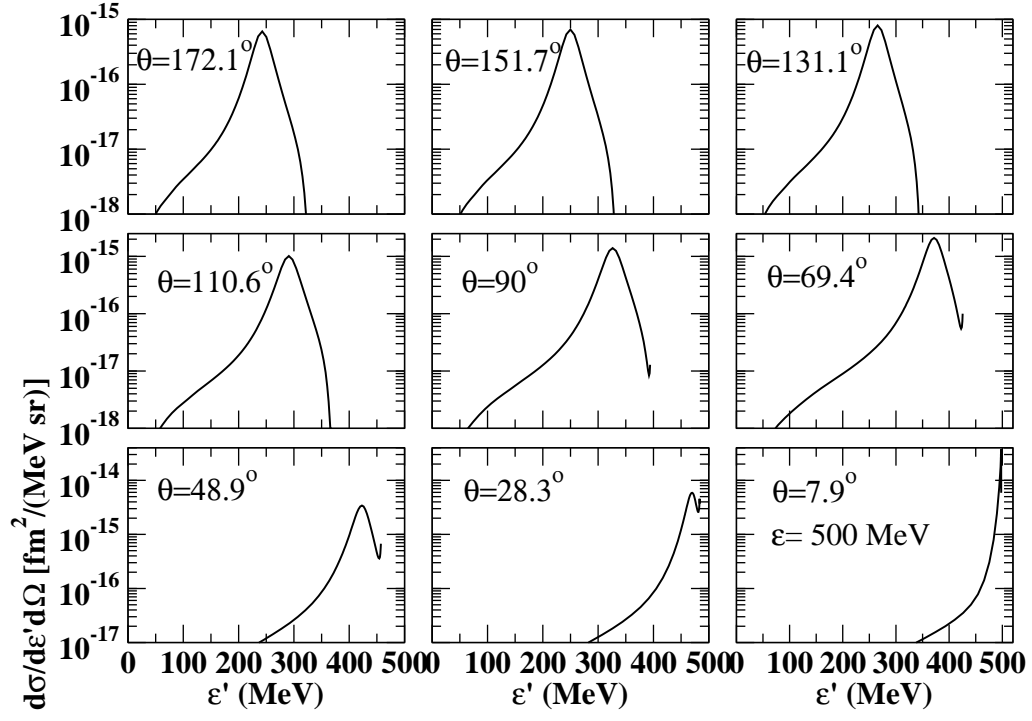


FIG. 13: Same as Fig. 12, but the incident neutrino energy is 500 MeV.

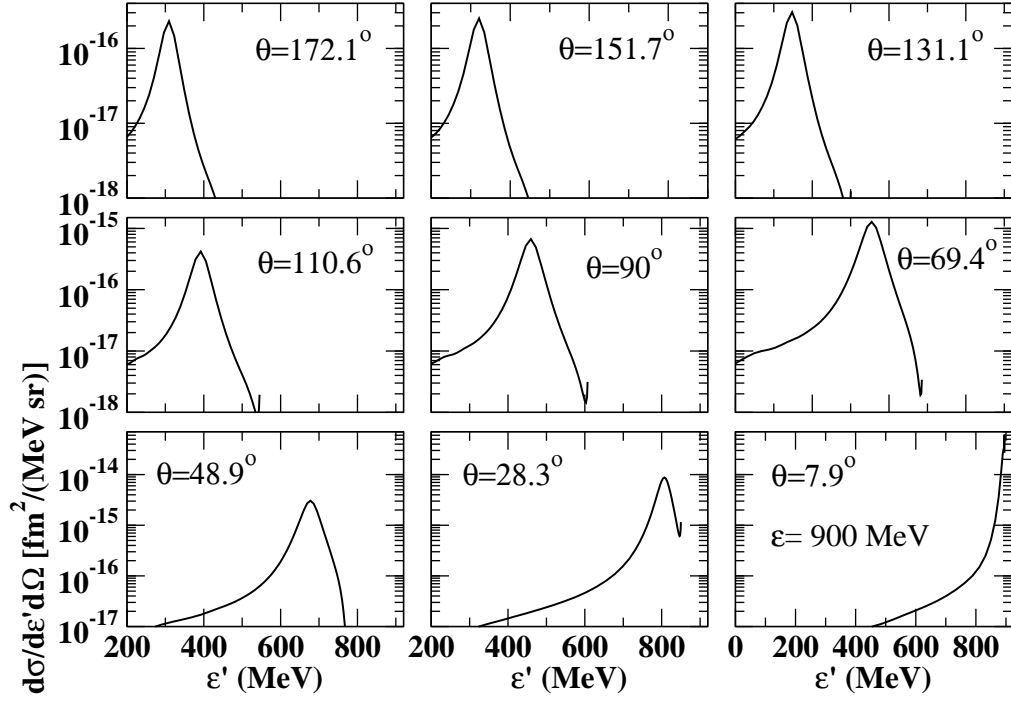


FIG. 14: Same as Fig. 12, but the incident neutrino energy is 900 MeV.

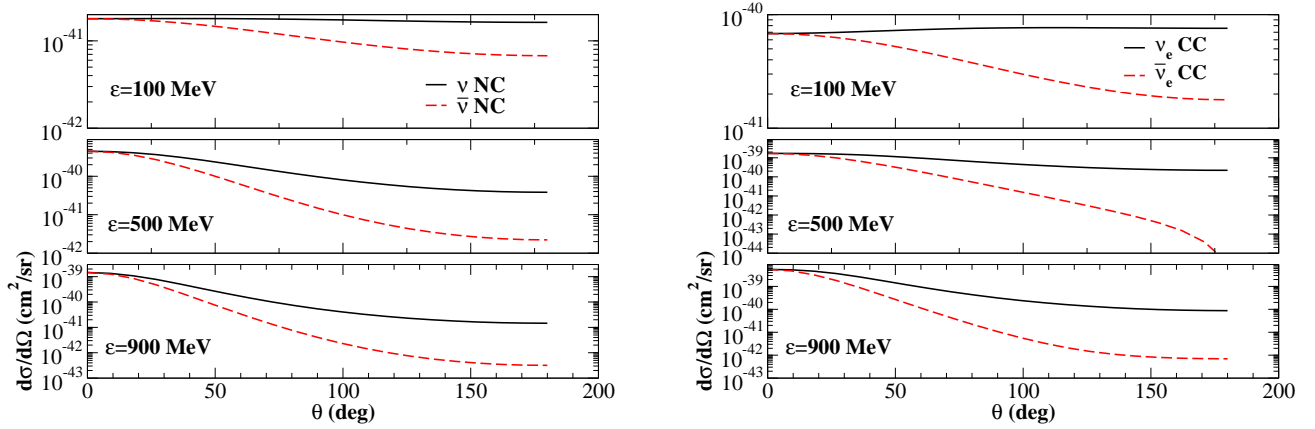


FIG. 15: (color on line) The “model” NC (left panel) and CC (right panel) differential cross sections for neutrino (solid lines) and antineutrino (dashed lines) energies of 100, 500, and 900 MeV, as functions of the final lepton scattering angle.

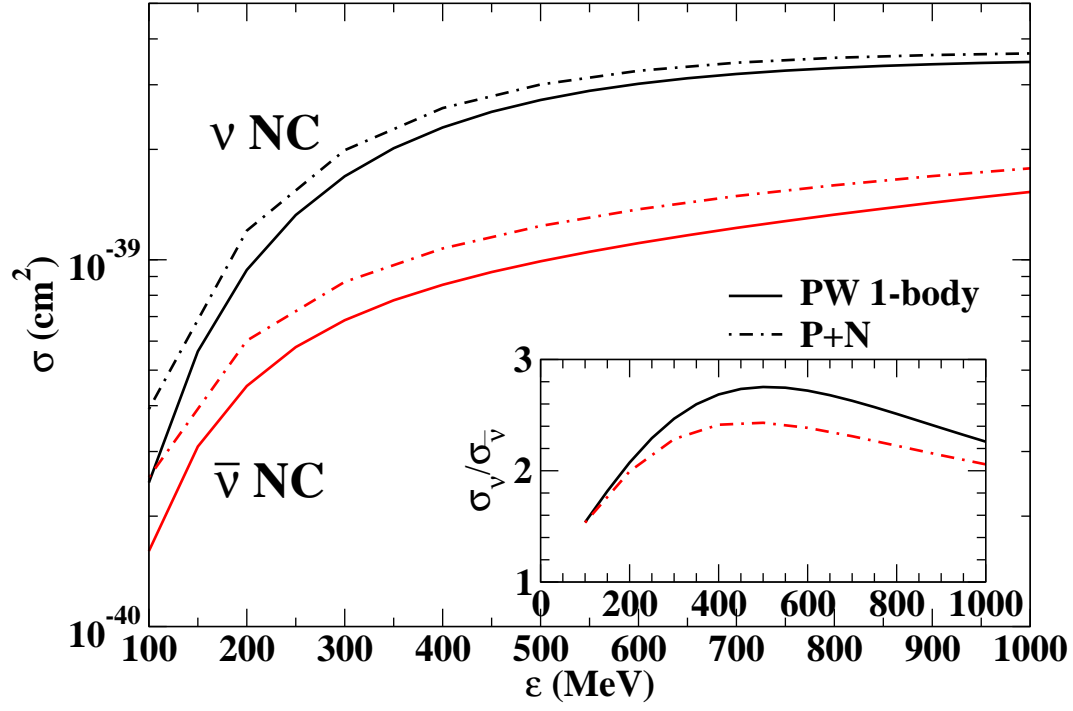


FIG. 16: (color online) The “model” (P+N) NC cross sections for neutrino and antineutrino are compared with plane-wave one-body (PW 1-body) results, see text for explanation. Inset: ratio of neutrino NC versus antineutrino NC cross section.

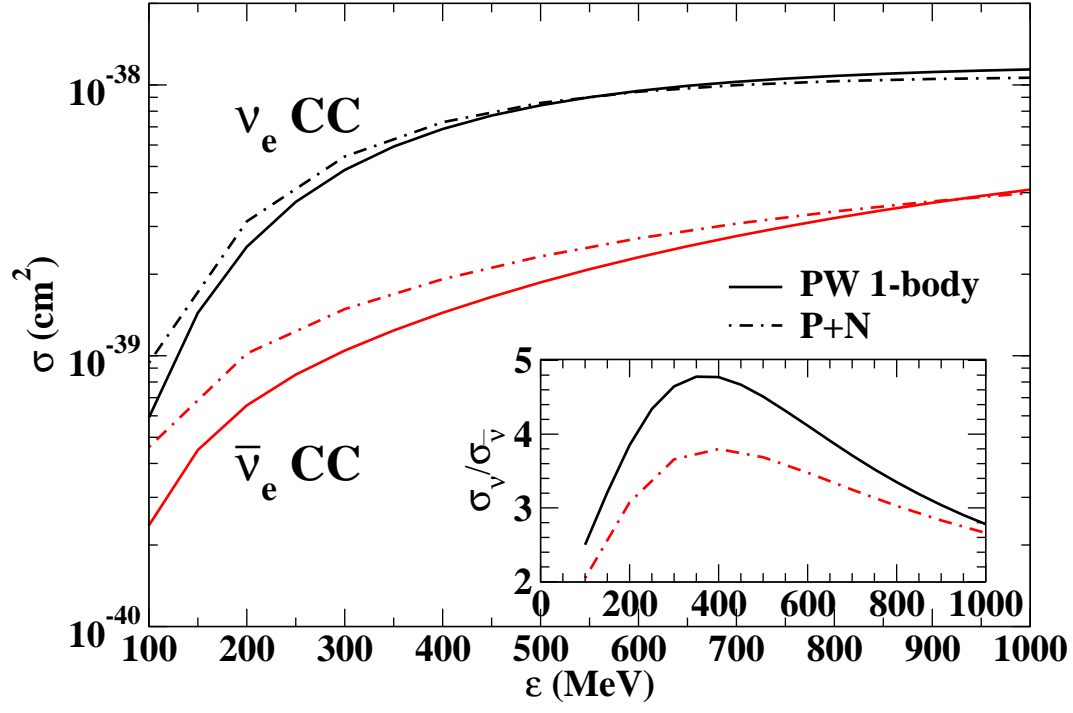


FIG. 17: (color online) Same as Fig. 16, but for CC cross sections.